May 2016

Room Temperature Gas Sensing Using Pure and Modified Metal Oxide Nanowires

Yale Wang
University of Wisconsin-Milwaukee

ROOM TEMPERATURE GAS SENSING USING PURE AND MODIFIED METAL OXIDE NANOWIRES

by

Yale Wang

A Thesis submitted in

Partial Fulfillment of the

Requirements for the Degree of

Master of Science

in Engineering

at

The University of Wisconsin-Milwaukee

May 2016

ABSTRACT

ROOM TEMPERATURE GAS SENSING USING PURE AND MODIFIED METAL OXIDE NANOWIRES

by

Yale Wang

The University of Wisconsin-Milwaukee, 2016
Under the Supervision of Professor Junhong Chen

Recently, various quasi 1D metal oxide semiconductor nanostructures (nanorods, nanowires, nanotubes, nanobelts) of various binary oxides have been found to be excellent materials for gas sensing. However, some of the sensitive gas sensors can work only at elevated temperatures. The sensing performance can be further improved when these oxides are doped with noble metal nanoparticles and form hetero-junction with other oxides, especially different types of metal oxide. These modifications can substantially change the surface properties as well as electronic properties due to their enhancement of the depletion layer at the metal nanoparticle-metal oxide nanowire and homo/hetero-interfaces.

The objective of this dissertation study is to investigate the sensing performance of WO_3, ZnO, NiO and TiO_2 nanowires towards various air pollutant gases such as NH_3, NO_2, H_2S and CO at room temperature. The sensing performance of pure metal oxide nanowires are further improved by doping these nanowires with noble metal nanoparticles and through the formation of n-p hetero-junction of two dissimilar oxides.

Based on this study, it was found that pure ZnO and NiO nanowires show a high sensitivity and the best selectivity performance towards the ppm level NO_2 (1 ppm) with respect to other interfering gases. On the other hand, both WO_3/Ag and WO_3-NiO gas sensors show enhanced

sensing and highly selective performance towards H_2S (~10ppm) at room temperature. Additionally, sensor response and recovery become faster with WO_3/Ag than pure WO_3 nanowires. The plausible reasons for such improvements with these surface modifications are discussed. This study provides a scientific foundation to engineer practical room-temperature gas sensors with enhanced performance.

TABLE OF CONTENTS

LIST OF FIGURES

LIST OF TABLES

LIST OF ABBREVIATIONS

HVAC	heating, ventilating and air conditioning
LOD	limit of detection
MFC	mass flow controller
MOS	metal oxide semiconductor
NP	nanoparticle
NW	nanowire
SEM	scanning electron microscopy
TLV	threshold limit value
WHO	World Health Organization
XRD	X-ray diffraction

ACKNOWLEDGEMENTS

I would like to first acknowledge my advisor, Prof. Junhong Chen, for his considerable guidance and patience during my Master's study at UWM. Being his student this one year has truly been a privilege and I would like to extend my thanks for everything he's done for me. It has been a wonderful experience to work and study in this group. I would also thank Sigma Aldrich for providing the metal oxide nanowires and Ag nanoparticles.

My sincere thanks are to Postdoc Shun Mao and Arnab Maity for their technical support with gas sensing area guidance. I thank Xiaoyu Sui for technical support with taking SEM images and Xingkang Huang for technical support on XRD analyses. I would also like to thank all the other members of my research group for their help.

I would like to thank my parents for their love and support; they are always standing by me throughout my life.

CHPATER 1 INTRODUCTION AND LITERATURE REVIEW

1.1 Background

Due to increasing vehicle and industrial emissions, there is a strong need for continuously monitoring the air quality in living and work places. Inhalation of various toxic gases such as H_2S, CO, NH_3 and NO_2 poses various instant and long term threats to human health. Therefore, an intelligent monitoring system is needed to supervise air quality and control heating, ventilating and air conditioning (HVAC) in order to ensure the maximum safety for the human life. Gas sensors are the heart of the system as they transduce the signal in the presence of toxic gases to the monitoring system that can recognize and send an alert signal to humans, both qualitatively and quantitatively or can give the feedback to HVAC to maintain a congenial atmosphere. Nanostructured metal oxide gas sensors are found to be a potential candidate as compared to other rivals such as chromatography and spectroscopy techniques due to their ease of use, simple fabrication, low cost and robustness. However, there are some issues such as poor selectivity, higher operating temperature and inadequate stability that limit their widespread application in various areas.

Recently, one-dimensional (1D) metal oxide nanowires/rods have become an interesting architecture that shows much better performance such as room temperature sensing, excellent sensitivity and selectivity with rapid response and recovery time [1-2]. They possess higher surface-to-volume ratio and congruence of the carrier screening length with their special one dimensional architecture that helps with efficient transduction of surface chemical processes into electrical signals [3-4]. To further improve sensing performance, sometimes various noble metals or various catalytic oxides are added on the host 1D metal oxide for a favorable gas adsorption/desorption process. The aim of this work is to study various metal oxide nanowire like

structures and the influence of composite hetero-structures towards dynamic gas sensing for various pollutants gases.

This chapter provides a short overview of the air quality monitoring with the current scenario, the working principle of metal oxide gas sensors, room temperature gas sensing with 1D metal oxide hetero-structures and various approaches found in the literature to improve the sensing performance. Based on the review, aims and work plans are identified for the thesis study.

1.2 Introduction

Large scale industrial and vehicle emissions of toxic gas pollutants have worsened air quality. Continuous respiration inside the stale cabin can induce far-reaching negative effects for mankind. Due to continuous industrial production, the greenhouse gases are emitted mainly from the burning of fossil fuels and lead to global warming. Various environmentally harmful gases including toxic and greenhouse gases such as H_2S, CO, NH_3, NO_2 and C_6H_6 can be present in the atmosphere. Table 1.1 shows a brief account of their source of production, toxicity and threshold limit value (TLV) as reported by the American Conference of Government Industrial Hygienists.

Table 1.1 The toxicity and source of listed air pollutant gases

Gas	Source of production	Toxicity to human	TLV	Ref.
H_2S	Mines, petroleum fields and natural gas production	Eye irritation and lung irritation, may cause death over 500 ppm	10 ppm	[5-6]
NH_3	Industrial refrigeration system and vehicle emissions	Eye, nose and throat irritation	35 ppm	[7]
CO	Fossil fuel incomplete combustion	Headache and dizziness, may cause death over 1600 ppm	25 ppm	[8-9]
NO_2	Vehicle emission and fuel burning	Eye, nose and throat irritation, may cause death over 100ppm	5ppm	[9]
C_6H_6	Petroleum products and building materials	Narcosis, eye irritation and skin irritation	2.5 ppm	[10]

TLV is defined as the maximum concentration of a chemical allowable for repeated exposure without producing adverse health effects. Reviewing Table 1.1, it is apparent that the limit of detection (LOD) of these gases by the sensors must be well below or at least equal to TLV. Therefore, there is a strong demand to develop a miniaturized air quality system for controlling HVAC to ensure optimum safety. Various techniques such as electrochemical, spectroscopic and chromatographic processes are followed to measure specific gas contents; however, they are time consuming, very costly, bulky and not suitable for real time applications. Metal oxide gas sensors (MOS) have significant advantages due to their small size, low cost and rapid detection process. The air quality monitoring system using MOS sensors consists of three basic segments including a "gas sensor" that changes its resistance in the presence of a toxic gas, "embedded hardware" that measures and stores the real-time data to the application processor, and "software" for analyzing and decision making about the contents of gas present in the atmosphere. Due to rapid advancements of recent electronics and computing technology, the last two segments (hardware and software) have already reached a satisfactory level; however, development of reliable MOS sensors still needs further research in order to improve their poor selectivity, stability and high operating temperature [11-13].

Various architecture and morphology (0D, 1D, 2D) have already been reported in gas sensing studies for different binary (ZnO, WO_3, SnO_2) and ternary oxides (AB_2O_4 or ABO_3). 1D nanostructures shows great advantages as compared to traditional thin film technology due to their higher surface-to-volume ratio, good stability for their excellent crystallinity, and excellent signal transduction in the presence of gaseous species for their less defective structures [14]. Additionally, due to the 1D structure, the surface catalytic activity is improved and promotes improved gas adsorption/desorption at room temperature. The performance is again further improved when these

oxides are doped with 0D catalytic noble metals (Ag, Pd, Au) and form hetero-junctions with other oxides [15]. These configurations (either with impregnated structure or composite hetero-junction) can substantially change the surface property as well as electronic property due to their enhancement of the depletion layer at the metal NP-metal oxide and homo/hetero-interface (n-n, n-p or p-p). Here, n and p stand for n-type and p-type MOS materials, respectively. The charge transfer occurs at the hetero junction due to their Fermi level adjustments and produces a large change in resistance (response %) upon gas exposure. These hetero-structures also change the acidity or basicity of the constituent oxides and improve the specific gas adsorption at the interface and thus improve selectivity [16].

In view of this, we have measured the gas sensing property of various 1D binary oxides (such as WO_3, ZnO, NiO and TiO_2). After that we modified the oxide surface with 0D noble metal (WO_3-Ag (1D-0D)) and also made n-p hetero junction (1D-1D) type ((n)WO_3-(p)NiO) to improve the sensing performance. We tested various toxic and combustible gases such as H_2S, NH_3, CO and NO_2 for optimizing the materials for selectivity. All sensing tests were carried out at room temperature to develop a heater-less MOS sensor unit. The special 1D structure shows excellent gas sensing performance at room temperature.

1.2.1 Air quality monitoring: current scenario

Nowadays, air pollution becomes a significant threat to human life due to continuous exposure to toxic gases and various pollutants from household sources and industrial and vehicle emissions. Continuous or instant inhalation in poor air quality, indoors and at various work places affects human life significantly by causing various health problems such as asthma, bronchitis and cancer. According to the 2014 WHO report, air pollution caused the deaths of around 7 million people

worldwide [17]. Recently in 2015, a significant red alert has been activated for air pollution due to hazardous air pollution levels in Beijing (20 times the limit recommended by WHO). Therefore, continuous and reliable monitoring of air quality is important in the current climate. The role of air quality monitoring instruments is to alert humans when the concentration of some toxic gas species crosses its toxicity limiting values (TLV). Presently, various techniques such as gas chromatography and optical spectroscopy are generally used for determining air quality, but as mentioned before, they are bulky, expensive, time consuming and trained persons are required to do the job. Therefore, a low cost, portable, power efficient gas analyzing system is in great demand. Nanostructured metal oxide gas sensors are found to be a promising alternative as they are low cost, smaller in size, rapid and robust in a corrosive environment. Some companies (such as Figaro and Honeywell) have successfully launched various gas detectors; however, they are power hungry (operated at high temperature), poorly selective, and show a very limited scope in various working areas. In this respect, significant research is in demand in the current air quality monitoring and market scenario to develop the sensors that can be operated in room temperature with high sensitivity, selectivity and reliability. With respect to current demand, the present study is focused on development and improvement of these parameters with various 1D binary metal oxides to detect various toxic gases such as, CO, NH_3, H_2S, C_6H_6 and NO_2. Practically, it is known that these gases can be present in a mixed gas environment. Therefore, they individually need to be selectively detected; otherwise, cross-selectivity can cause a false alarming from the measuring system.

1.2.2 Characteristics of metal oxide gas sensors

Gas sensors are devices that can transform the chemical signature of an analyte gas into an electronic signal and are one of the important components of "electronic nose" technology. The electronic conductivity of metal oxide semiconductors varies with the composition of the gas atmosphere surrounding them.

The working principle of the gas sensors is schematically shown in Figure 1.1[18]. The oxygen molecules extract electrons from the conduction band E_c and then become adsorbed oxygen anions on the surface of metal oxide grains. This will lead to a band bending and a depletion area called the space charge area. Once the target gas molecules reach the surface and boundary of the metal oxide grains, they will react with the oxygen anions and change the electron concentration in the metal oxide materials. This will lead to the conductivity change and become the electronic signal that can be observed.

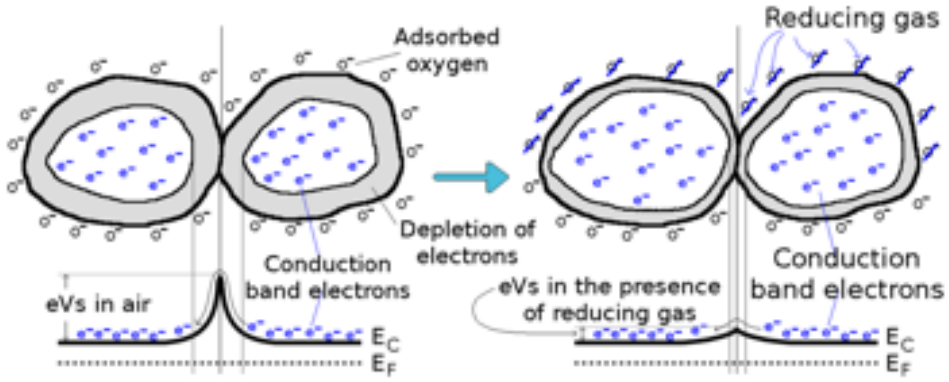

Figure 1.1 Structural and band models of conductive/sensing mechanism upon exposure to a reducing gas. [18]

The sensing mechanism in metal oxide gas sensors is related to ionosorption of species over their surfaces. When the gas sensor is exposed in ambient oxygen, the adsorbed oxygen ion will be formed with the oxygen molecules extracting the electrons from the metal oxide inside.

Nitrogen dioxide is known as a kind of oxidizing gas that will react with the oxygen ion and keep the electrons at the surface. That means the electron concentration in the metal oxide will decrease. Since the majority of carriers in n-type MOS are electrons, the conductance of n-type MOS will decrease after being exposed to NO_2. For the p-type MOS gas sensor, the majority of carriers are holes. The extracted electron will increase the concentration of holes inside. So this means the conductance of p-type MOS will increase after being exposed to NO_2.

NH_3, H_2S and CO are all reducing gases in our ambient environment. When the gas sensor is under the ambient reducing gas, the electrons obtained from the chemical reaction in the adsorbed oxygen ion forming process are given back to the conduction band as indicated in Figure 1.2 below. For the n-type MOS sensor, these electrons will increase the carrier concentration and lead to a decrease in the sensor resistance. For the p-type MOS sensor, the electrons go back into the valence band and recombine with the holes, which results in reducing the concentration of holes and leads to an increase in the sensor resistance.

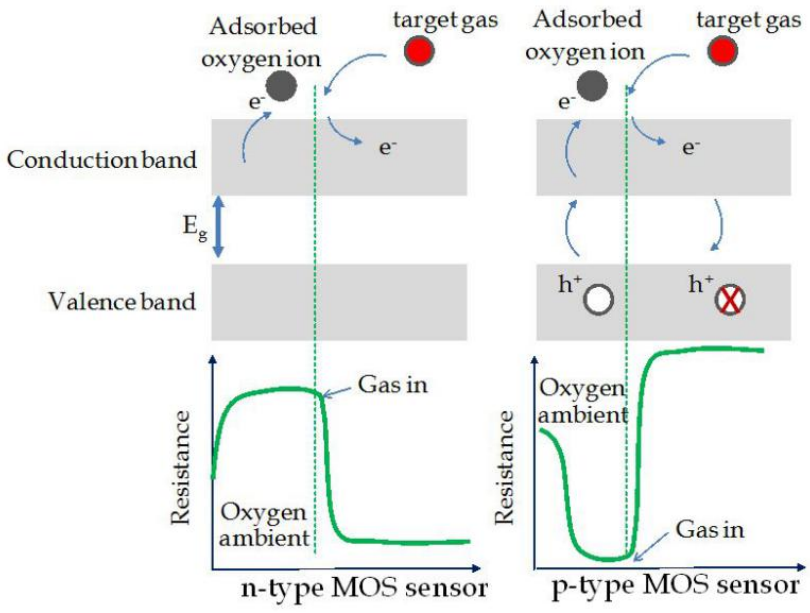

Figure 1.2 Schematic diagram for change of the sensor resistance upon exposure to the target gas (reducing gas) in the case of n-type and p-type MOS sensors. [59]

The set of parameters to characterize the sensing performance of the metal oxide gas sensors are shown in Table 1.2.

Table 1.2 Definition of gas sensing characteristics

Sensitivity(S)	Change of measured signal per analyte concentration unit. In this thesis, the mathematical expression used is $$S = \frac{\left\|(R_a - R_g)\right\|}{R_a} \quad (1.1)$$ where R_a stands for the sensor resistance in the air and R_g stands for the sensor resistance in the carrier gas containing target gases.
Selectivity	The capability of the gas sensor to respond to one specific target gas mixed with other gases. Eq 1.2 describes the selectivity of the gas sensor for a target gas (a) relative to another gas (b) with the same concentration $$\text{Selectivity} = \left\|\frac{R_a - R_{ga}}{R_a - R_{gb}}\right\| \quad (1.2)$$ where R_a stands for the sensor resistance in air and R_{ga} and R_{gb} stand for the steady sensor resistance in specific gases, respectively.
Response time	The time for the current reach the 90% of the final change in current after the sensor is exposed to the target gas.
Recovery time	The time for the current to recover the 90% of the maximum change in current once the target gas is turned off.

1.3 Literature review

1.3.1 Metal oxide nanowire gas sensor application: state-of-the-art research

The first generation of MOS gas sensors were prepared by a thick film technology. The materials fabrication processes have been improved towards thin film technology because reduction of crystallite size caused a significant improvement in gas sensor performance. Recently, various quasi 1D MOS nanostructures (nanorods, nanowires, nanotubes, nanobelts) of various binary oxides are found to be excellent materials as compared to thick and thin film

technology for gas sensing as they provide uniform crystalline structures with well-defined chemical composition, higher surface area with better catalytic properties, free from dislocation and defects, good stability etc.[19] Additionally, 1D nanomaterials are easy to prepare and have excellent signal transduction properties from the gas-solid interaction. Nanowires have been defined as wires with at least one spatial dimension in the range of 1-100 nm. In 1991 Yamazoe [20] indicated that the reduction of crystallite size caused a significant improvement in gas sensor performance. The gas sensing performance will be enhanced remarkably when the diameter of nanowires (D) is close to or less than double the thickness of the space-charge layer (2L). For D < 2L, the main part of the metal oxide grain or the whole grain is depleted of electrons. The sensor resistance is very sensitive to sensing effect in this case. As Figure 1.3 [21] indicates, the charge depletion layer is produced during the adsorbed oxygen molecules trapping the electrons from metal oxide to the surface. The thickness of the charge depletion layer (L) has a positive correlation with the potential conductivity variation of the metal oxide gas sensor, so the best situation is that the metal oxide grain is fully depleted.

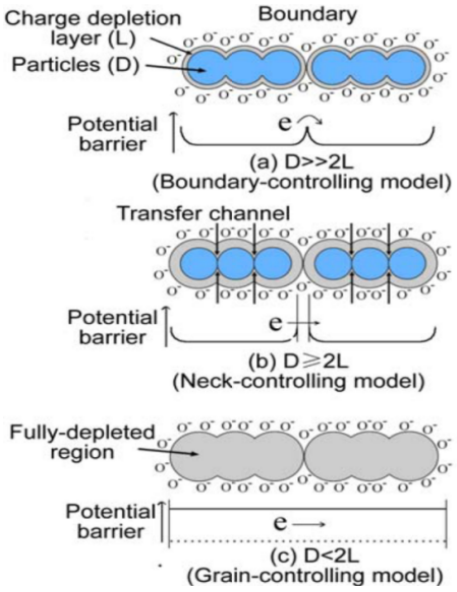

Figure 1.3 Schematic model of the effect of the crystallite size on the sensitivity of metal oxide gas sensors. [21]

Table 1.3 Literature papers focusing on the sensing properties of metal oxide gas sensors.

Target gas	Material	OT(℃)	S $\lvert(Ra-Rg)/Ra\rvert$	Concentration	Size (nm)	Ref.
H_2S	ZnO Nanorod	RT	30%	1ppm	50	[22]
H_2S	ZnO Nanowire	RT	25%	4 ppm	100-200	[23]
H_2S	CuO Nanowire	RT	80%	100ppm	80-200	[24]
H_2S	ZnO Thick film	300	25%	12ppm	1000-5000	[25]
H_2S	TiO_2 Nanoparticle	350	210%	200pm	50-60	[26]
NO_2	SnO_2 Nanoribbon	RT	700%	100ppm	80-120	[27]
NO_2	WO_3 Nanowire	300	70%	50ppb	200	[28]
NO_2	TiO_2 Nanofiber	300	800%	500ppb	200-500	[29]
NO_2	ZnO Nanobelt	350	75%	10ppm	10	[30]
NO_2	ZnO Nanorod	250	400%	10ppm	10-20	[31]
CO	CeO_2 Nanowire	RT	100%	200ppm	50	[32]
CO	SnO_2 Nanowire	200	30%	12ppm	>100	[33]
CO	WO_3 Nanowire	200	100%	50ppm	160-300	[34]
NH_3	ZnO Thick film	350	600%	1000ppm	Thick film	[35]
NH_3	WO_3 Nanowire networks	400	100%	30ppm	200	[36]
NH_3	NiO Nanowire	400	20%	50ppm	150	[37]

Table 1.3 summarizes the recent work in the 1D MOS nanostructure for the gas sensing study. From Table 1.3, it is clear that, although these nanostructures show some excellent response towards specific gases, their operating temperature is very high. If compared at room

temperature and corresponding TLV limit, the response % is very small. Therefore, significant improvement is needed to achieve a room temperature sensor. Various strategies are being investigated to improve the performance and are discussed in the next section.

1.3.2 Strategy for improvement of gas sensing performance

Surface decoration with noble metal nanoparticles is a powerful method for enhancing gas sensing characteristics. Noble metal additives such as Pd [38], Pt [39], Au [40], Ag [41-42] and Cu [43] on an oxide surface or in its volume have been investigated for a long time. The promoting effects of noble metals have been widely confirmed in semiconductor gas sensors (Table 1.4). The working principle of dopant for enhancing the sensing performance of pure metal oxide could be explained in two main effects: the spillover effect and the catalytic effect. The most understandable explanation is the additive metal nanoparticles would increase the metal oxide surface coverage of the gas during a spillover process (Figure 1.4). The oxygen in air could form oxygen anions while reacting with not only the metal oxide but also the dopant. That increases the gas-solid interaction and response.

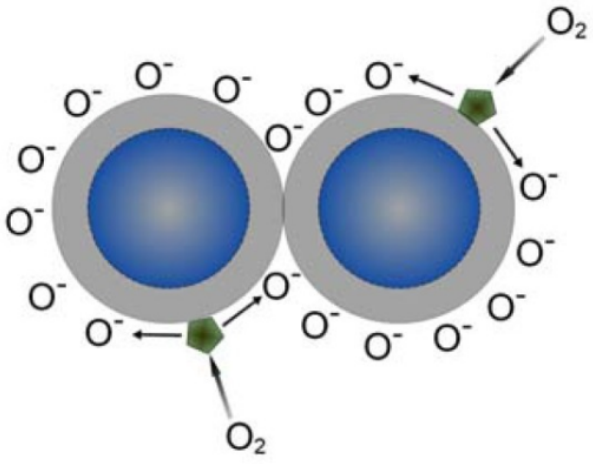

Figure 1.4 Schematic model of oxygen spill over process on the surface of doped metal oxide

Table 1.4 Literature papers focusing on the improvement of sensing properties by noble metal doped metal oxide gas sensors.

Target gas	Material	OT(℃)	S $\lvert(Ra - Rg)/Ra\rvert$	Concentration	Size (nm)	Ref.
CO	ZnO-Au	350	30%	5ppm	100	[44]
CO	ZnO-Pd	300	350%	100ppm	80	[45]
NO_2	SnO_2-Ru	75	4000%	200ppm	100-900	[46]
H_2S	SnO_2-Ag	RT	40%	3ppm	Thick film	[47]
H_2S	SnO_2-Sb	RT	15%	50ppm	50-80	[48]
C_6H_6	ZnO-Ag	330	300%	100ppm	25-35	[49]
NH_3	WO_3-Cr	300	90%	500ppm	20	[50]

Recent studies indicated that the characteristics of metal oxide gas sensors could also be improved through the use of composite metal oxides [51-53]. The physical interface between two dissimilar materials with different band gap and work-function is often referred to as a hetero-junction. The material incorporation of these two components is known as a hetero-structure [54]. A hyphen between compounds (e.g. "WO_3-NiO") represents a simple mixture of the two constituents, being mostly randomly distributed throughout the material. The easiest way to obtain metal oxide composites is by simple mechanical mixing of oxide powders.

Depending on the carrier type (n/p type), a composite hetero-junction can be formed with similar types (n-n, p-p) or dissimilar types (n-p). Once the p-n junction is formed at the connect boundary of the p-type and n-type metal oxide grain, the different band gap of the two metal oxides will induce the band to bend to equalize the Fermi level, and a depletion layer will be formed due to mutual charge transfer. This will decrease the width of the charge conduction channel and increase a large potential barrier between the two grains. Thus, a larger change in

resistance occurs in the presence of gases and thereby shows enhanced sensitivity. In Table 1.5 we summarize work on the sensing properties of metal oxide hetero-structure gas sensors.

Table 1.5 Literature papers focusing on the sensing properties of metal oxide hetero-structure gas sensors

Target gas	Material composite	OT(℃)	S |(Ra-Rg)/Ra|	Concentration	Size (nm)	Ref.
CO, C_6H_6	ZnO NiO	450	200%	5ppm	30-70 10-40	[55]
H_2S	ZnO CuO	100	4000%	100ppm	90-200 30	[56]
NH_3	ZnO Cr_2O_3	RT	13.7%	300ppm	400 2000	[57]
NO_2	ZnO Eu_2O_3	300	1600%	3ppm	200 50	[58]

1.4 Organization of thesis

The main research objective of this dissertation is to investigate the gas sensing characteristics of the metal oxide nanowires at room temperature and the tunability of sensing performance of these gas sensors through decorating their surface with various nanoparticles.

Chapter 1 presents the background introduction and literature review about the state-of-the-art metal oxide gas sensors.

Chapter 2 includes all the experimental details applied in the thesis and structural characterization of the metal oxide nanowire materials.

Chapter 3 presents the sensing performance of pure ZnO, WO_3, NiO and TiO_2 nanowires against target gases.

Chapter 4 focuses on the tuning sensing performance through silver doping and p, n type metal oxide nanowire mixing, analysis of the sensing results, and discussion of the sensing mechanism.

Chapter 5 presents a summary of this thesis and recommendations for future studies.

CHAPTER 2 FABRICATION AND CHARACTERIZATION OF GAS SENSORS

2.1 Fabrication of gas sensors

This chapter describes the fabrication of unmodified and modified MOS nanowire (WO_3, NiO, TiO_2, ZnO) based gas sensor devices and various characterization techniques with their working principles to evaluate the micro-structure and phase information. For the modification of the surface of nanowires, silver nanoparticles were used to coat the WO_3 nanowire. Additionally, we have prepared a hetero-junction nanostructure ((n) WO_3-(p) NiO) to further improve the sensing performance. All the chemicals are purchased from Sigma-Aldrich and used without further purification. In the following sections, the fabrication details of the MOS nanowire gas sensor device are described.

2.1.1 Fabrication of pure metal oxide nanowire gas sensors

Interdigitated gold electrodes were fabricated using e-beam lithography on a silicon substrate with a SiO_2 thin top layer. DI water was used as the solvent applied for these metal oxide nanowires. The concentration of the pure metal oxide nanowire dispersion was 3g/L. NWs were first uniformly dispersed in DI water by ultra-sonication. Then, a tiny drop of the nanowire dispersion was drop casted on the gold electrode, and the metal oxide nanowires bridged the gold fingers after the solvent evaporation. After deposition, the pure metal oxide nanowire sensors were annealed at 200 ℃ for 1h in Ar flow (1 lpm) to improve the contacts between the nanowires and the gold electrodes. The schematic of the electrodes and sensor devices is indicated in Figure 2.1 below.

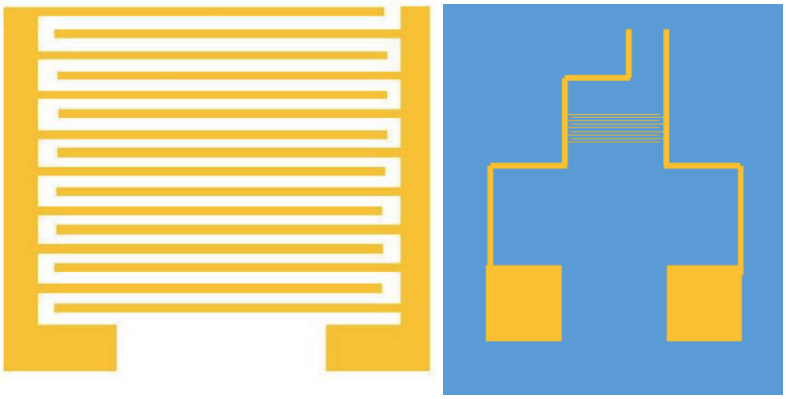

Figure 2.1 Schematic of electrodes and sensor devices

2.1.2 Silver-decorated tungsten oxide nanowire gas sensors

Ag nanoparticles were provided by Sigma Aldrich. The Ag nanoparticle in stock was suspended in isopropanol (IPA). The concentration of tungsten oxide nanowires was 0.01M and three different concentration of Ag NPs (such as 0.001M, 0.0001M and 0.00001M) were prepared and mixed with the WO_3 nanowire solution. After mixing, all the WO_3/Ag samples were ultra-sonicated for 40 minutes. The resulting solutions were drop casted on a gold electrode on the Si/SiO_2 substrate. The post annealing treatment was kept the same as mentioned before.

2.1.3 Fabrication of (n)WO_3- (p)NiO nanowire hetero-junction mixed composite gas sensors

To prepare the x WO_3– (1-x) NiO (where $0 \leq x \leq 1$) hetero-junction, the individual nanowire samples were prepared in the same concentration (0.01 M) as discussed in the earlier section. Then they were separately mixed in three different volume ratios such as 3:1, 1:1 and 1:3. After that, ultra-sonication was followed by drop-casting and the annealing condition was maintained in the same manner to prepare pure and composite series (pure WO_3, W3N1, W1N1, W1N3 and pure NiO).

2.2 Micro-structural characterization of nanowires by scanning electron microscopy

Scanning electron microscopy (SEM) can produce images of a sample by scanning it with a beam of high energy electrons. The layout and function of SEM are shown as Figure 2.2 [60]. A beam of electrons is generated by an electron gun, processed by magnetic lenses, focused at the specimen surface and systematically scanned across the surface of the specimen. The images are not the real image of the samples. They are in the form of secondary electron signals, which comes from the electron-sample interactions. The SEM images can indicate the morphology and topography of samples.

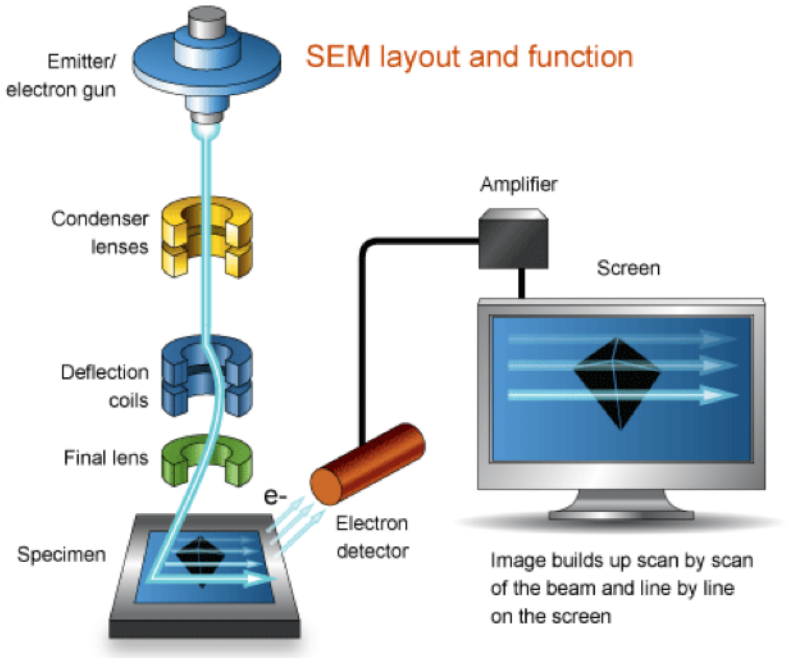

Figure 2.2 Schematic illustration of the layout of SEM [60]

Scanning electron microscopy (SEM) was carried out to investigate the average diameter and length of these nanowires. We used the electrode covered with nanowire dispersion for the SEM imaging. Figure 2.3 shows the SEM image of the TiO_2 nanowires. As can be seen, the

diameter of a single nanowire was 10 nm and the length of nanowires ranged from 400 to 700 nm.

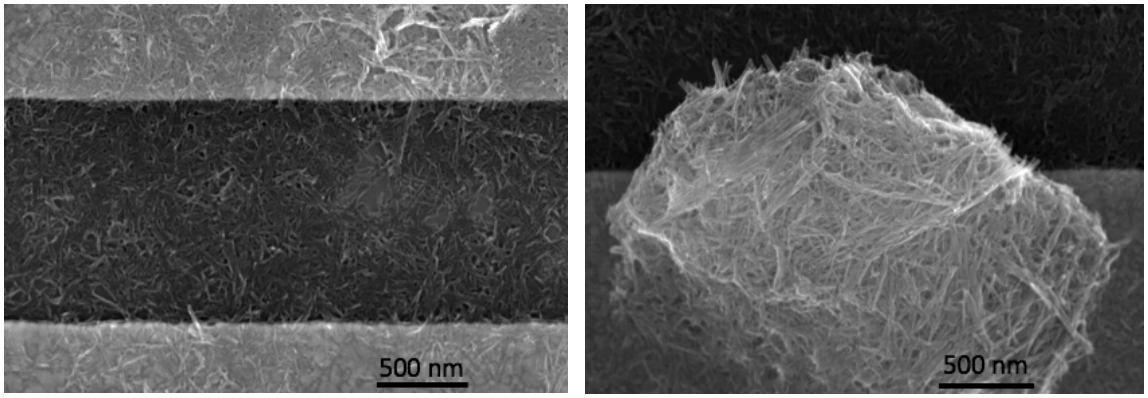

Figure 2.3 SEM images of pure TiO_2 nanowires.

Figure 2.4 is the SEM image of the pure WO_3 nanowires deposited on the gold electrodes. From the picture, we could see that the diameter of the nanowires varied from 50 to 80nm and the length was between 3 and 7μm.

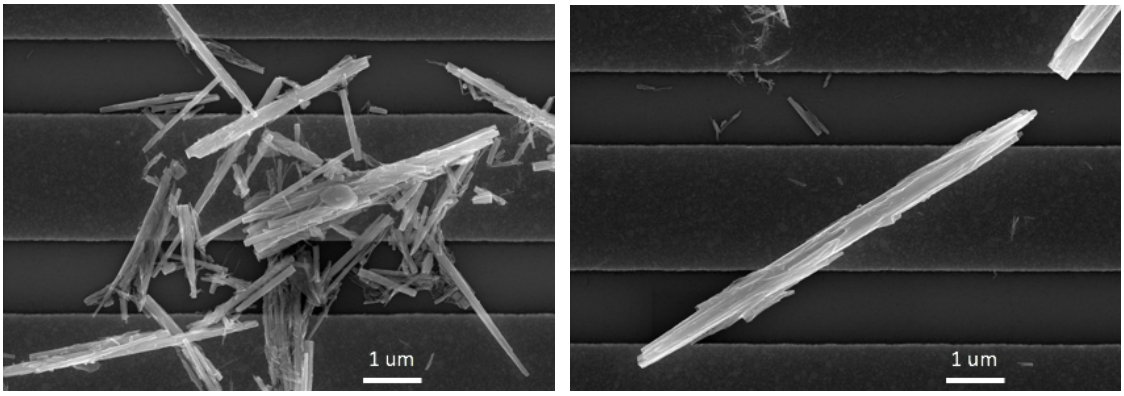

Figure 2.4 SEM images of pure WO_3 nanowires

Figure 2.5 shows the SEM images of pure NiO nanowires. The diameter ranged from 10 to 30 nm. The length of nanowires varied from 100 to 500 nm.

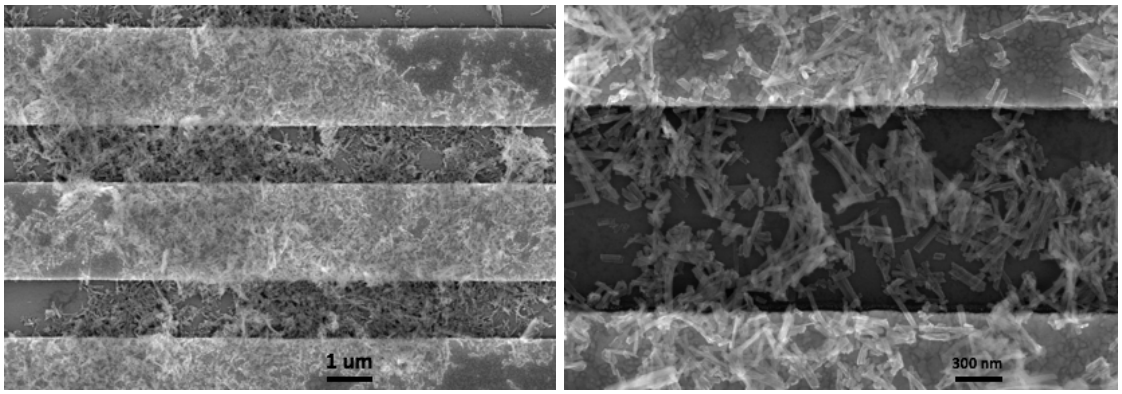

Figure 2.5 SEM images of pure NiO nanowires

Figure 2.6 shows the SEM images of pure ZnO nanowires. From the images, we could see that the diameter of this nanowire was around 50-80 nm and the length was about 400-600 nm.

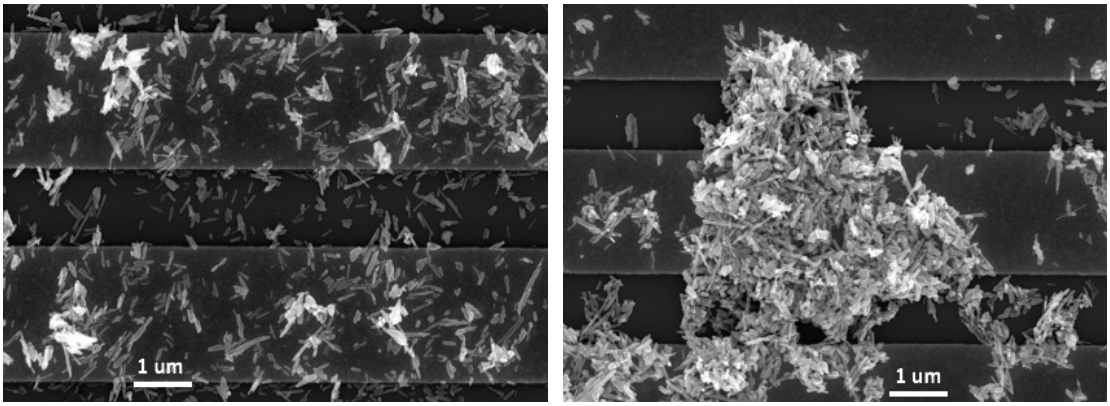

Figure 2.6 SEM images of pure ZnO nanowires

2.3 Phase information study by XRD technique

2.3.1 Working principle of XRD

The crystallographic structure of these pure metal oxide nanowires was characterized by powder X-ray diffraction. X-ray powder diffraction (XRD) is an analytical technique widely used for phase identification of a crystalline material and can provide information on unit cell dimensions. Crystals of materials are regular arrays of atoms, and X-rays can be considered waves of electromagnetic radiation. Atoms scatter X-ray waves through the atoms' electrons

known as the scatterer. A regular array of scatterers produce a regular array of spherical waves. Although these waves cancel one another out in most directions through destructive interference, they add constructively in a few specific directions, determined by Bragg's law. By scanning the sample through a range of 2θ angles, all possible diffraction directions of the lattice could be attained due to the random orientation of the powdered material. Since most materials have unique diffraction patterns, compounds can be identified by using a database of diffraction patterns.

The instrumentation of powder X-ray diffractometer is indicated in Figure 2.7 [61]. A powder X-ray diffractometer consists of an X-ray source (usually an X-ray tube), a sample stage, a detector and a way to vary angle θ. The X-ray is focused on the sample at some angle θ, while the detector opposite the source reads the intensity of the X-ray it receives at 2θ away from the source path. The incident angle is then increased over time while the detector angle always remains 2θ above the source path.

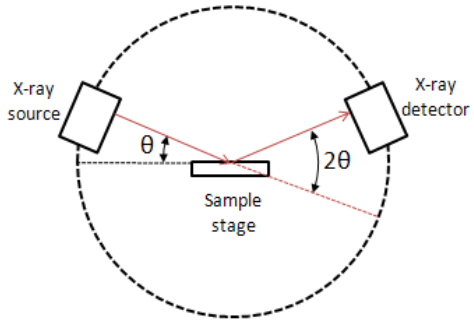

Figure 2.7 Schematic illustration of the instrumentation of powder X-ray diffractometer. [61]

2.3.2 XRD results and analysis

The XRD test results of these metal oxide nanowire powders are shown in Figure 2.8. In Figure 2.8a, the peaks were weak and broad, suggesting the poor crystallinity of the NiO

nanowires. Figure 2.8b indicates that the WO_3 was as the major phase while the minor impurity was detected as indicated by the XRD peaks at 14.8˚ and 29.8˚. The impurity phase could be $WO_3 \bullet 5H_2O$, which requires more information to confirm; for example, the elements related to the compounds to prepare the WO_3. Figure 2.8c is the XRD results of pure ZnO nanowires. No impurity phase was detected. Figure 2.8d shows the TiO_2 is not an anatase or rutile, but could be TiO_2-B.

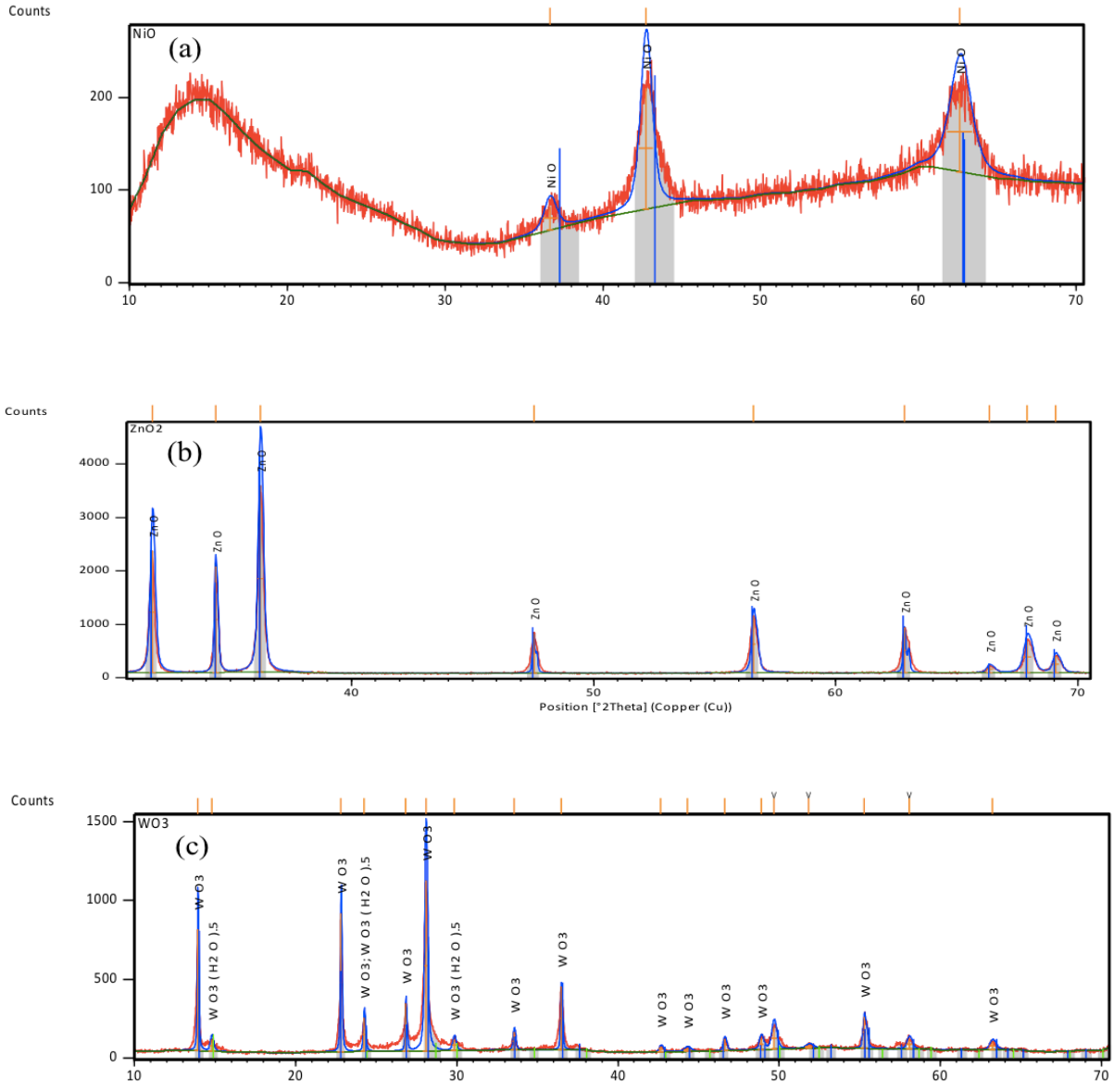

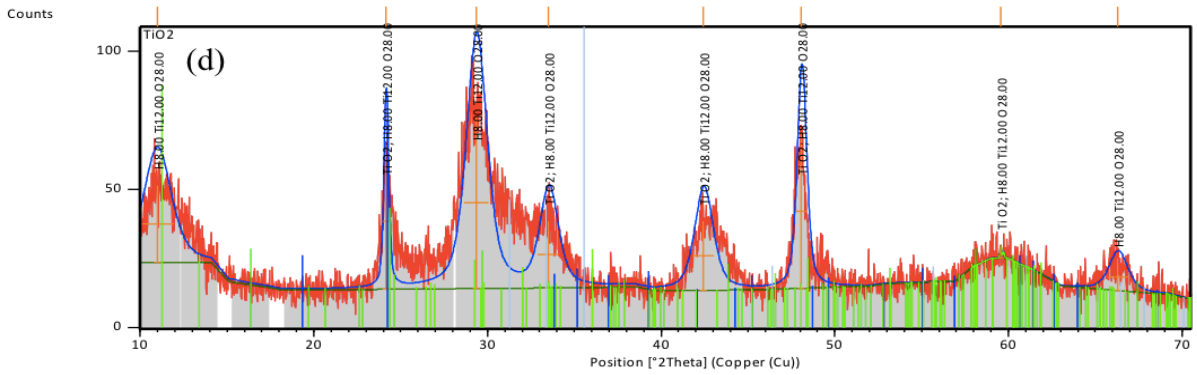

Figure 2.8 XRD results images of (a) NiO, (b) WO_3, (c) ZnO, (d) TiO_2.

2.4 Dynamic gas sensing system and sensing measurement procedure

Figure 2.9 shows the structure of the gas sensing test system applied in my thesis. This system consists of a sensing test chamber, a Keithley source meter (2602, Keithley, Cleveland, Ohio), and two flow meter connected to air and testing gas, respectively.

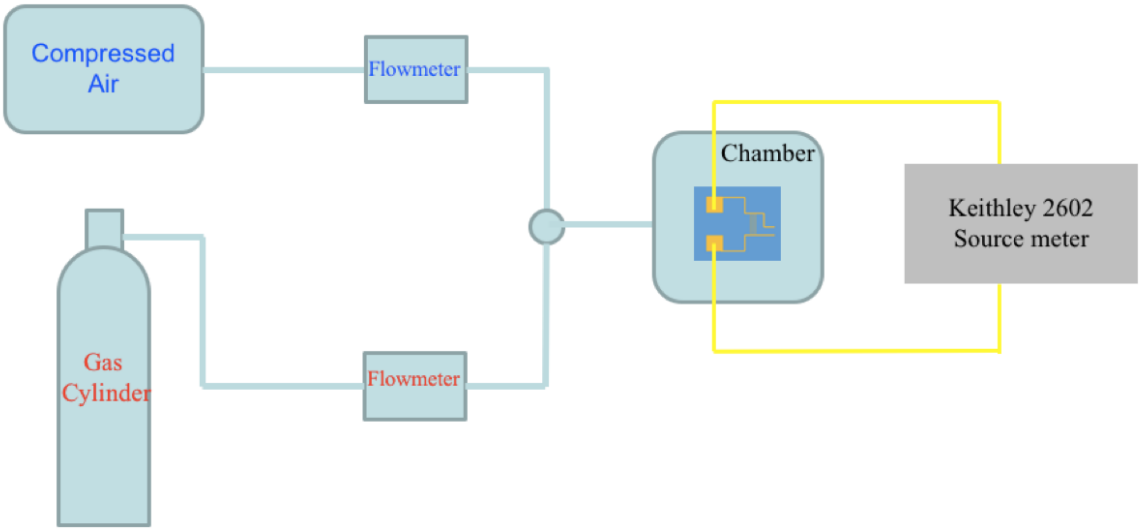

Figure 2.9 Schematic illustration of sensing test system used in the sensing experiment

At first, a sensor was placed into an air-tight test chamber connecting with electrical feedthroughs. Then a constant dc voltage was applied to the electrode connected by nanowires or

nanowire composites. The Labview 7.1 program was applied in sensing test for controlling the Keithley 2602 source meter. Figure 2.10 is the screen shot of operational interface of the Labview program. One typical gas sensing test cycle had three continuous steps: First, a clean compressed dry air flow was introduced into the sensing chamber as the baseline of the whole test. Normally, the preset time for this step is 10 minutes or even longer till the baseline of current becomes stable. Second, the different target gases diluted in air were injected through the flowmeter into the test chamber with the same flow rate as the first step to generate the sensing signal. The exposure time for the target gas was 5 minutes. Finally, the target gas was turned off and clean air was introduced again for sensor recovery for 10 minutes. The program setting for concentration control is also indicated in the Figure 2.10 labeled as MFCs. The words ending with "min" represent the setting for the first and last steps. The setting words ending with "max" means the setting for the second step. The setting number for the air flow rate is just the same as the number we put in, but the real flow rate of the target gas has a transfer relation ($F_R = F_s * 25$ mlpm) with the number indicated on the screen. For example, if we set the flow rate same to Figure 2.10, that means in the first and last steps of the sensing cycle, only the air (2 lpm) was introduced into the chamber. In the second step, the flow rate of air was 1.8 lpm as indicated and the flow rate of the target gas was 8*25=200 mlpm, which means the concentration of testing target gas was diluted into one tenth of the concentration in stock.

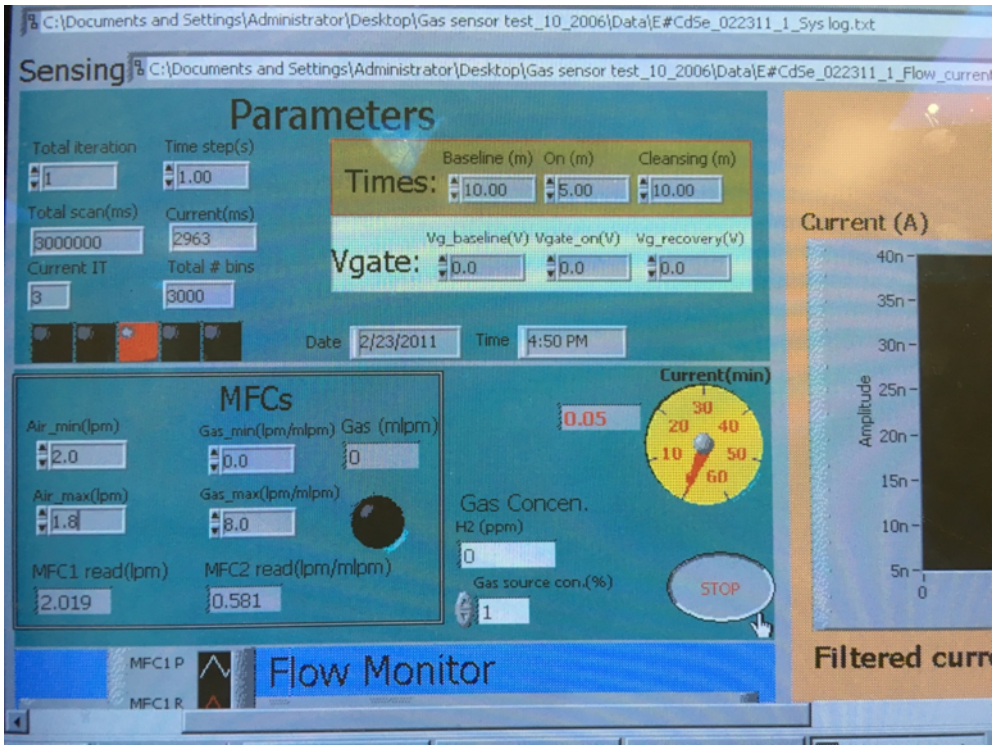

Figure 2.10 Screen shot of operation interface/control panel of the Labview gas sensing test program

2.5 Summary and conclusion

We have obtained and characterized pure NiO, ZnO, WO_3 and TiO_2 nanowires using SEM and XRD. The SEM results demonstrate that all the pure metal oxide materials are 1D nanowires. The XRD test results demonstrate good crystallinity of these nanowires except for NiO. We have also fabricated the modified nanowires (e.g. WO3/Ag and (n)WO_3-(p)NiO). The dynamic gas sensing test results of these fabricated nanowire devices are discussed in the next chapter.

CHAPTER 3 GAS SENSING PERFORMANCE OF PURE METAL OXIDE NANOWIRES

3.1 Introduction

To investigate the gas sensing properties of the synthesized metal oxide semiconductor nanowires, various toxic gases (NO_2, NH_3, H_2S, CO) were selected. As mentioned in Chapter 1, these gases can be present in work areas in an outdoor/indoor environment and can show various harmful effects to the human body. Therefore, they need to be detected well below their TLVs. We also have repeated testing for at least two sensors for each nanostructure and sensing test condition, which makes the results more reliable and repeatable. All the gas sensing measurements are done at room temperature.

3.2 Gas sensing results of various reducing and oxidizing gases

3.2.1 Nitrogen Dioxide (NO_2)

The dynamic response of different bare metal oxide (NiO, ZnO, TiO_2, WO_3) semiconductor nanowires to 1 ppm NO_2 at room temperature are shown in Figure 3.1. The respective responses of these sensors are 58.7% (NiO), 66.7% (ZnO), 50.4% (WO_3), and 60.1% (TiO_2) respectively. NO_2 is an oxidizing gas and the current will increase for p-type MOS sensor and decrease for n-type MOS sensors as the electrons are taken away from the sensing surface. The sensing mechanism of NO_2 can be expressed by Reaction 3.1 and 3.2 as follows:

$$NO_2(gas) + e^- \leftrightarrow NO_2^- (ads) \quad (3.1)$$

$$NO_2(ads) + O_2^- + 2e^- \leftrightarrow NO_2^- (ads) + 2O^-(ads) \quad (3.2)$$

The observed response is rapid for ZnO (~160 s) and NiO (~220 s) but slower for WO_3 (~270 s) and TiO_2 (~280 s). As shown in the Figure, the recovery for all these sensors is sluggish and can

not completely recover in 10 minutes; however, NiO and ZnO show comparatively better recovery among all sensors.

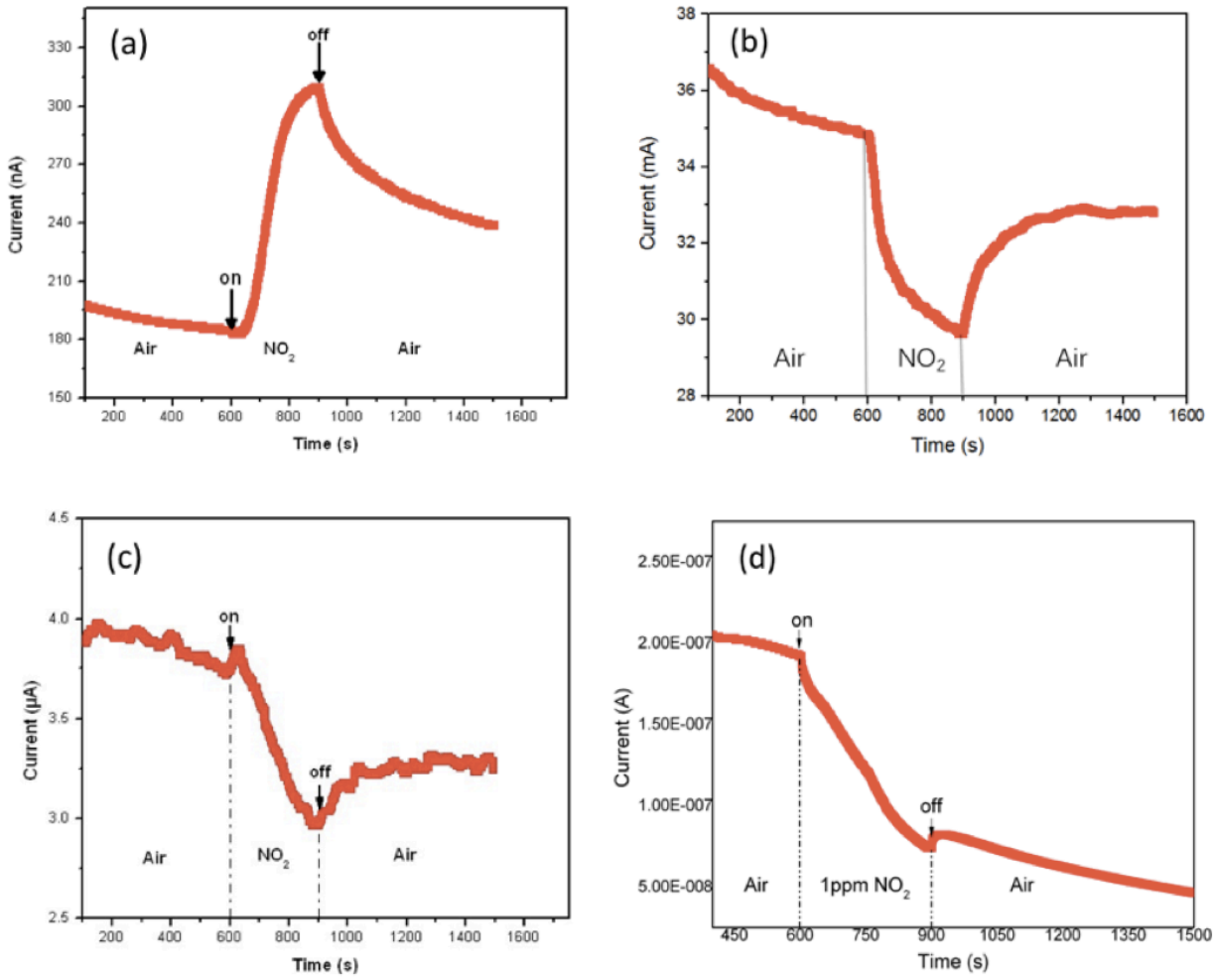

Figure 3.1 Dynamic response and recovery curve of 1 ppm NO_2 for (a) NiO, (b) ZnO, (c) WO_3 and (d) TiO_2.

3.2.2 Ammonia (NH_3)

The dynamic response to reducing gas NH_3 (100 ppm) at room temperature are shown in Figure 3.2 (a) NiO, (b) ZnO, (c) WO_3 and (d) TiO_2. Ammonia is a reducing gas and therefore,

the current will decrease for p-type MOS sensors and increase for n-type MOS sensors. The sensing mechanism of metal oxide nanowires towards NH_3 gas is described by Reaction 3.3:

$$4NH_3 + 3O_2^- = 6H_2O + 2N_2 + 3e^- \quad (3.3)$$

The average responses towards NH_3 for these metal oxides are 9.5% (NiO), 11.7% (ZnO), 37.5% (WO_3) and 97.5% (TiO_2), respectively. From the Figure, it is apparent that all four MOS sensors exhibit a fast response. These metal oxide nanowires also show faster recovery and better reversibility except for NiO nanowires.

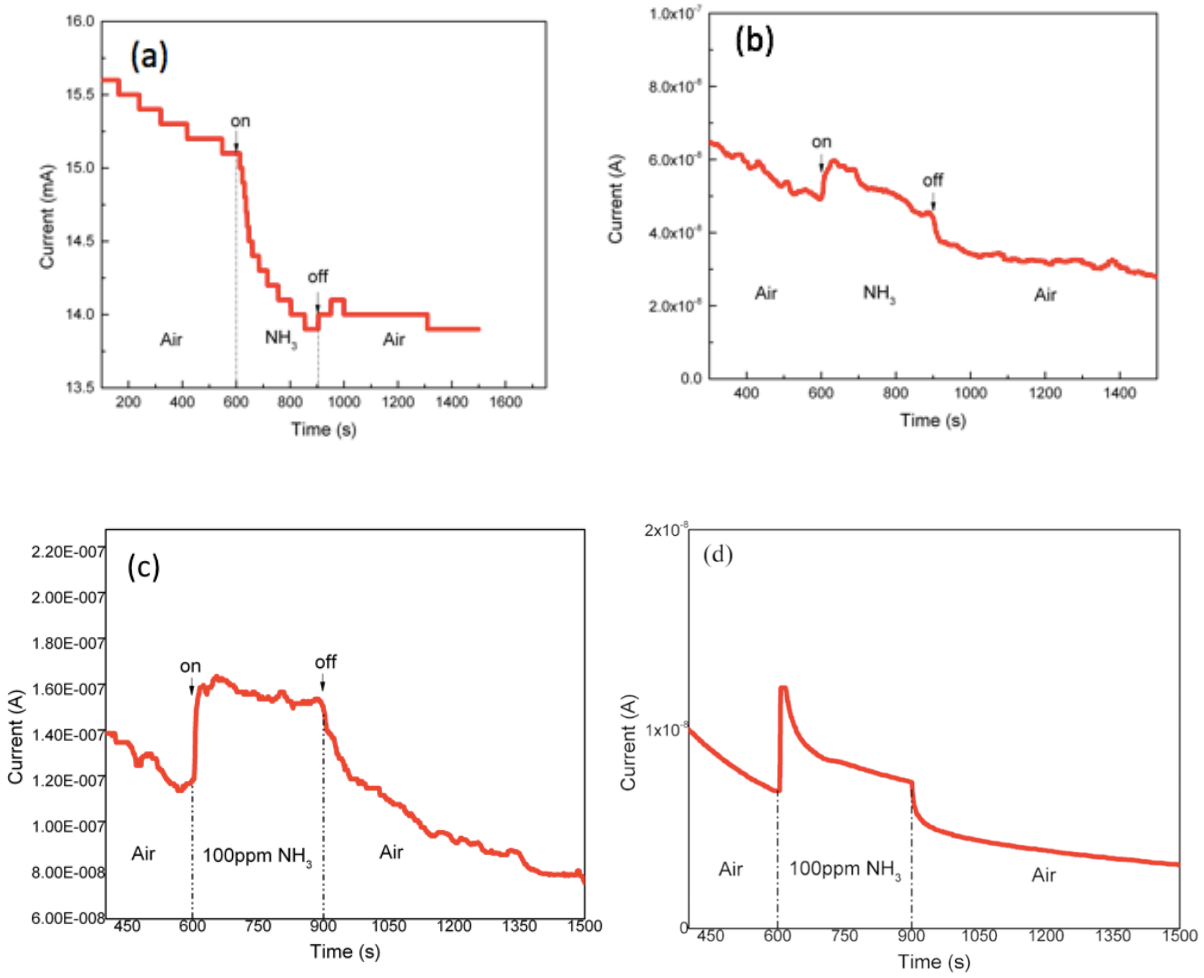

Figure 3.2 Dynamic response and recovery curve of 100 ppm NH_3 for (a) NiO, (b) ZnO, (c) WO_3 and (d) TiO_2.

3.2.3 Hydrogen Sulfide (H_2S)

Hydrogen sulfide is a colorless toxic and flammable reducing gas. The sensing mechanism of H_2S gas is given by Reaction 3.5, which describes the surface reaction with adsorbed oxygen species and release of electrons:

$$2H_2S + 3O_2^- = 2H_2O + 2SO_2 + 3e^- \quad (3.4)$$

Figure 3.3 shows the 10 ppm H_2S sensing performance for (a) NiO, (b) ZnO, (c) WO_3 and (d) TiO_2 but only WO_3 shows a reasonable response % (50%) among all sensors. The WO_3 nanowire gas sensor shows a fast response (~50 S) and recovery (~130 S) and is reversible in nature.

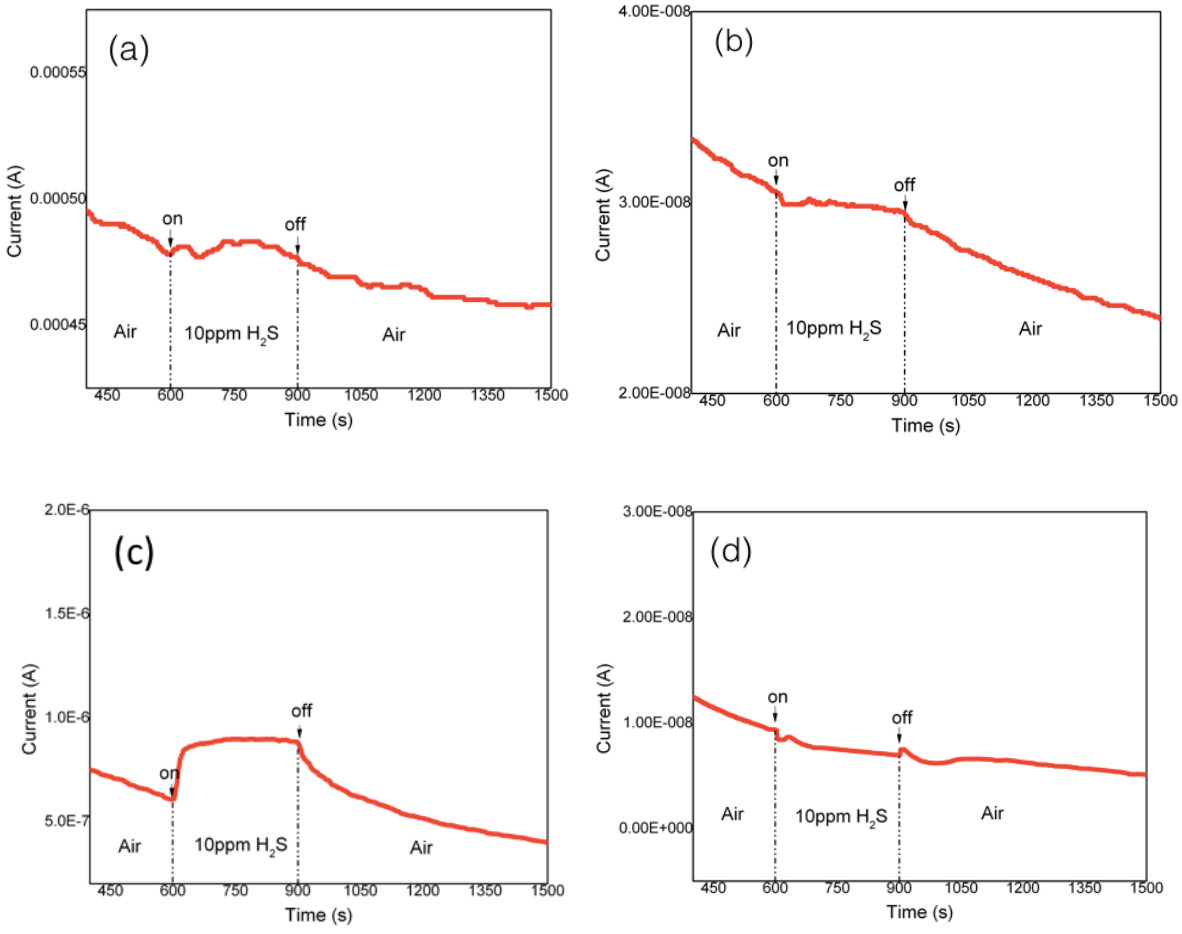

Figure 3.3 Dynamic response and recovery curve of 10 ppm H_2S for (a) NiO, (b) ZnO, (c) WO_3 and (d) TiO_2.

3.2.4 Carbon Monoxide (CO)

CO is a colorless and toxic reducing gas. Sensing response is suggested to be based on the CO oxidation reaction:

$$2CO + O_2^- = 2CO_2 + e^- \quad (3.5)$$

As a result, the surface oxygen concentration is reduced, and electrons that were initially trapped by oxygen anions are released.

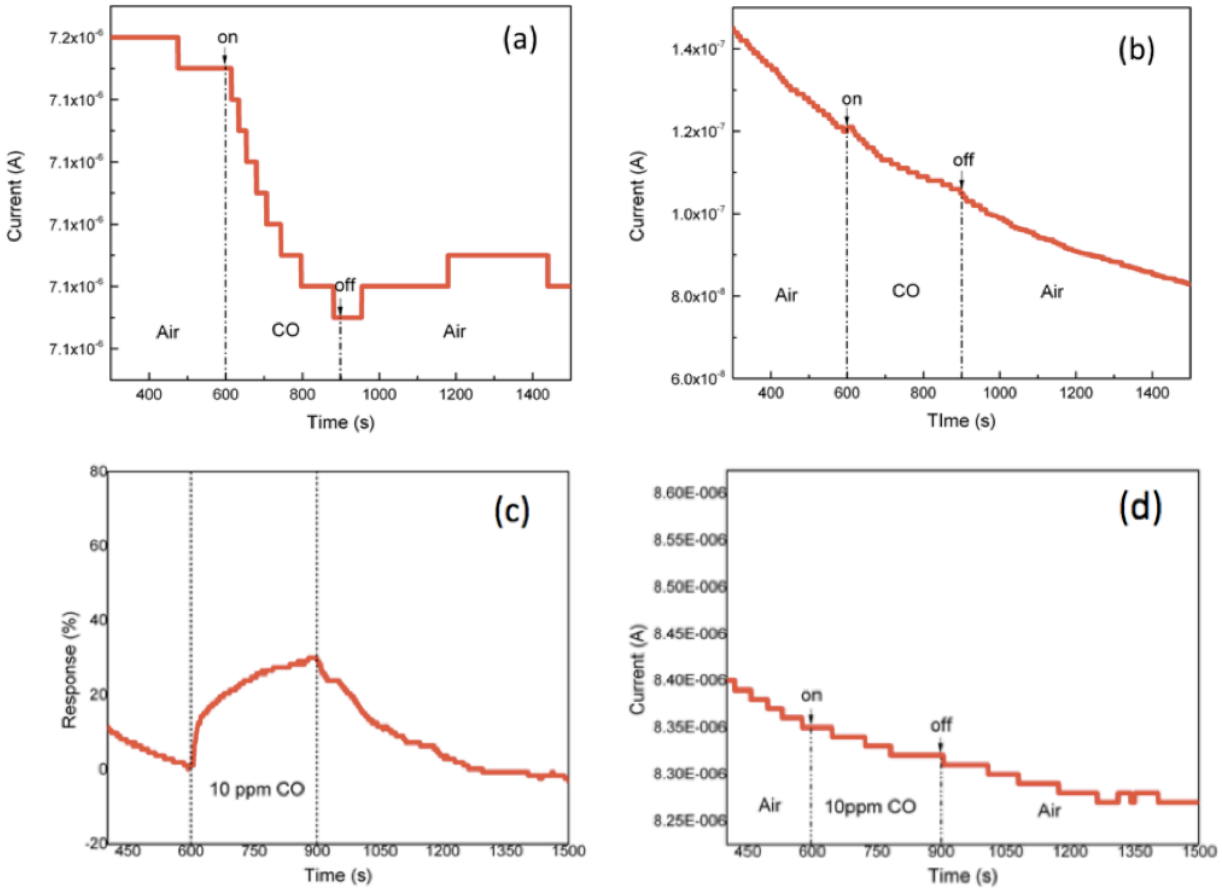

Figure 3.4 Dynamic response and recovery curve of four MOS to 10 ppm CO (a) NiO, (b) ZnO, (c) WO_3, (d) TiO_2.

From the gas sensing performance, it is found that only WO_3 shows significant response against CO. As shown in Figure 3.4, the response % of WO_3 nanowires after exposure to 10 ppm

CO is about ~38%. The response % of other metal oxides (NiO, ZnO and TiO_2) towards 10 ppm CO is <~ 5%. The response and recovery time for WO_3 is ~150s and ~270s respectively.

3.3 Comparison of gas sensing performance for selectivity study

Figure 3.5 shows the comparative gas sensing performance of sensors for (a) WO_3, (b) TiO_2, (c) ZnO and (d) NiO nanowires. It is apparent that WO_3 shows a good response and poor selectivity towards all target gases. The TiO_2 nanowire shows the best sensing performance to NO_2 and negligible response to CO and H_2S; however, cross selectivity can not be avoided towards NH_3. NiO and ZnO both exhibit good sensitivity and selectivity towards NO_2 as compared to the other interfering gases.

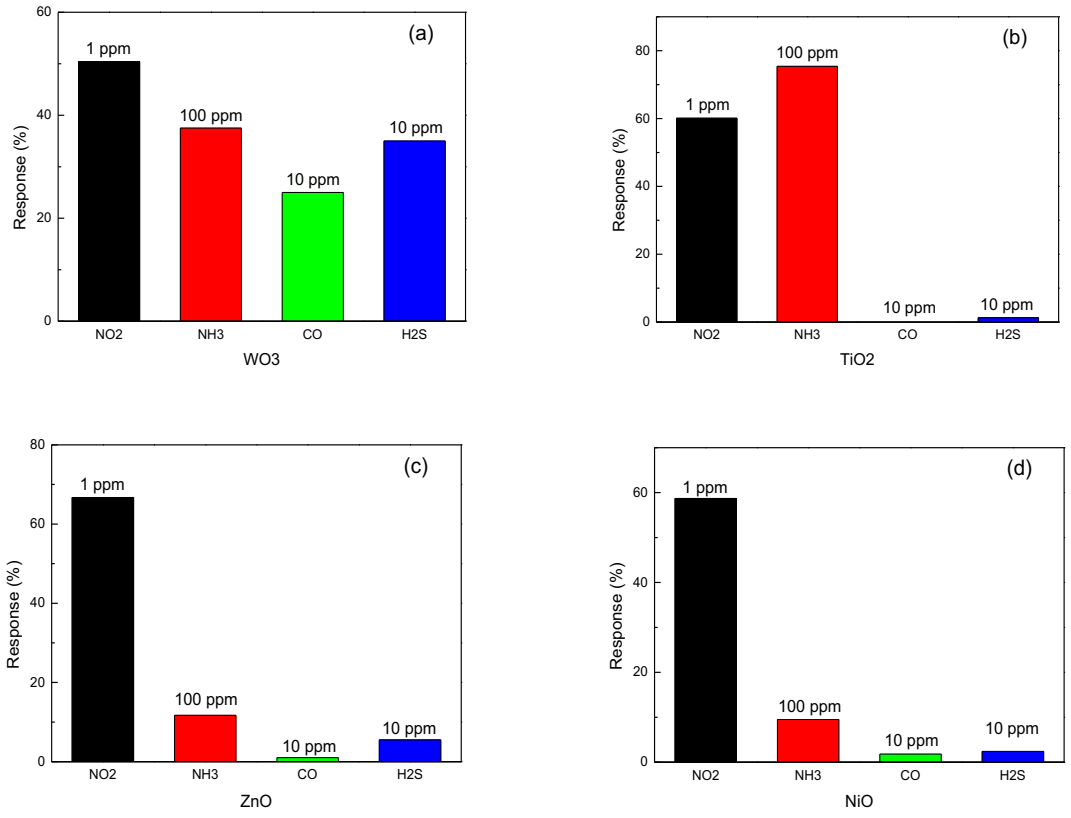

Figure 3.5 Summary of gas sensing performance for (a) WO_3, (b) TiO_2, (c) ZnO, (d) NiO.

3.4 Summary and conclusion

In this chapter, the gas sensing performance of four metal oxide nanowires at room temperature for NH_3, NO_2, CO and H_2S has been demonstrated. We have also identified the best sensing materials with respect to sensitivity and selectivity from their response behavior. For example, it is found that ZnO and NiO show the optimum response towards the sub ppm level (~1 ppm) NO_2 and there is almost negligible interference from other high concentration gases (~100 ppm NH_3 and 10 ppm of CO and H_2S). For the recovery process, these metal oxides indicated slow recovery performance under most sensing situations. This may be due to the room temperature operation, as the operating room temperature is not high enough for metal oxide surface to desorb the target gas molecules from the sensing surface to ambient environment. However, a comparatively better performance is observed over most of the reported sensors as indicated in Chapter 5. To further improve the performance and to find better selectivity for other gases such as H_2S, the MOS nanowire samples are further modified with noble metals/hetero-junctions and are discussed in the next chapter.

CHAPTER 4 TUNING SENSING PERFORMANCE OF METAL OXIDE NANOWIRES

4.1 Introduction

This chapter demonstrates the gas sensing properties of nanowires modified by noble metals and hetero-junctions. In the previous chapter, we showed excellent response and selectivity towards NO_2 with ZnO or NiO nanowires. However, it is also required to sense other toxic gases such as H_2S (well below their TLV), as they can also be present in the same working environment. We have selected WO_3 nanowires for surface modification as it shows cross selectivity to other gases. However, WO_3 nanowires themselves exhibit a maximum response (~40%) towards H_2S as compared to other metal oxide nanowires (< ~1%).Therefore, it could be interesting if we can improve the H_2S gas sensing performance with respect to sensitivity and selectivity. In the following sections we describe the gas sensing performance of Ag NP-decorated WO_3 and hetero-junction of (n)WO_3-(p) NiO.

4.2 Silver nanoparticles-decorated WO_3 nanowire gas sensing

The fabrication of silver-doped WO_3 nanowire gas sensor was introduced in Chapter 2.

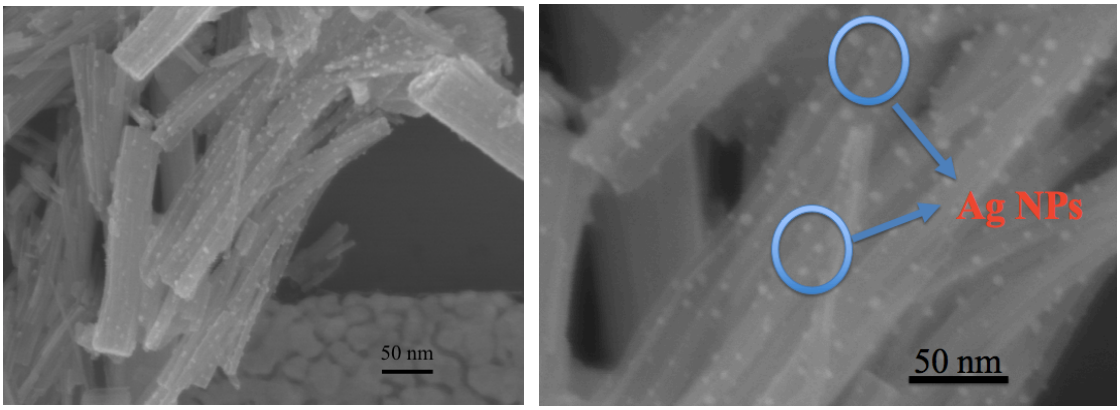

Figure 4.1 SEM images of Ag doped WO_3 nanowires

Figure 4.1 shows SEM images of the sensor with Ag NP loadings. It is observed that the Ag nanoparticles are dispersed and decorated uniformly on the WO_3 nanowires.

The dynamic sensing responses of bare WO_3 NWs and WO_3/Ag with various molar ratios towards 10 ppm H_2S are shown in Figure 4.2. From the Figure, it is found that as the molar ratio of silver increases, the response% also increases until the molarity of Ag NPs reaches 0.0001M. After that, the response diminishes for higher silver amounts. Thus, maximum sensing performance comes from 0.0001M Ag-decorated WO_3 NWs gas sensor. The results demonstrate that the sensitivity increased from 39±0.5% for bare WO_3 to 75±0.3% for WO_3/Ag (molar ratio 100:1) with the same exposure time, which clearly indicates the significant sensing enhancement in the presence of Ag NPs (see Figure 4.2b). It is also to be noted that response and recovery becomes faster for the silver doped sample than pure WO_3. For example, response time becomes smaller for the optimized 0.0001M Ag-doped WO_3 sample (~95 s) compared with the pure WO_3 sample (~275 s).

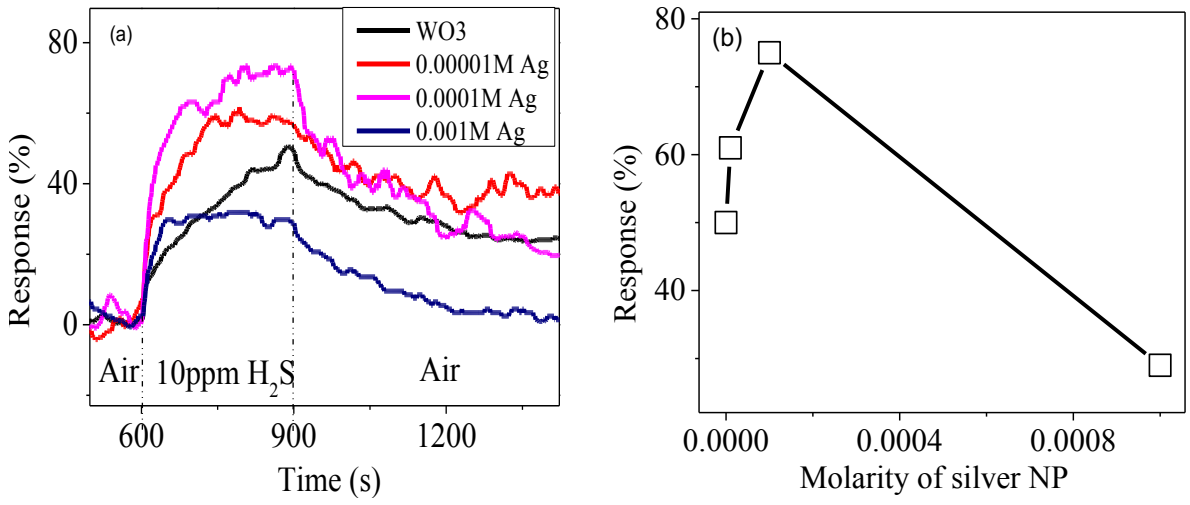

Figure 4.2 (a) Dynamic response of bare WO_3 NWs and WO_3/Ag to 10ppm H_2S and (b) response % vs silver molar amount.

The improved response of Ag-doped WO_3 gas sensor towards H_2S can be explained as follows. Firstly, Ag nanoparticles are known to be catalytically active, and therefore, they can promote more active atomic oxygen by dissociating the less active molecular oxygen. Thus Ag nanoparticles can enhance the gas molecule adsorption on the surface and accelerate the electron exchange between the metal oxide gas sensor and the target gas. Secondly, Ag has a different work function, and when it comes to the WO_3 surface, it forms nano-schottky junction and thus modulates the electronic conduction path with a barrier height enhancement. This produces a large change in resistance in the presence of gas. For higher molar concentration of Ag, the conductivity mechanism is significantly controlled by the metallic nature of silver and thus sensitivity drops at a higher molar ratio of Ag NP. Figure 4.3 indicates the model of Ag doping influence on WO_3 nanowire. The red line is the conductivity path through Ag-doped WO_3 sensors.

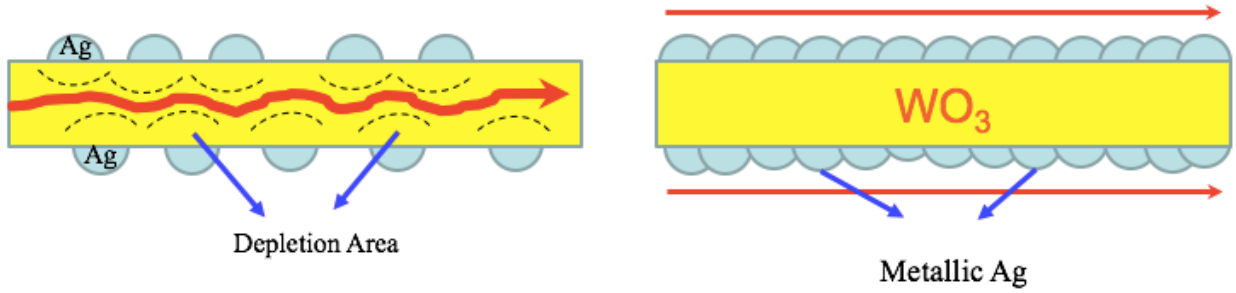

Figure 4.3 Schematic model illustration of Ag doping influence on the electronic conductivity path in Ag-doped WO_3 sensors.

4.3 WO_3-NiO nanowire composite sensing results and discussion

The easiest way to obtain metal oxide composites is by simple mechanical mixing of existing oxide powders. We have fabricated the composite nano structure of diode like hetero junction of 'n' type WO_3 and 'p' type NiO in different molar ratio, namely pure WO_3, W3N1(molar ratio of WO_3 to NiO is 3 to 1), W1N1(molar ratio of WO_3 to NiO is 1 to 1), W1N3

(molar ratio of WO_3 to NiO is 1 to 3) and pure NiO. The details of the synthesis parameters were discussed in Chapter 2.

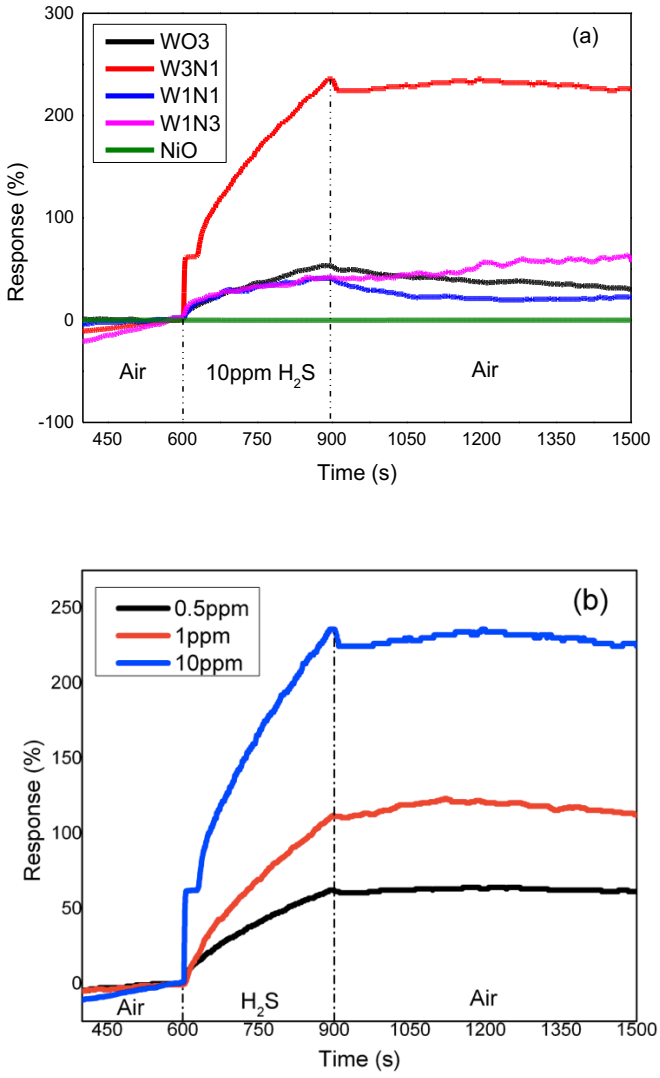

Figure 4.4 (a) Dynamic response and recovery curve of WO_3-NiO nanocomposites. (b) Dynamic response of the W3N1 nanocomposites to 0.5 ppm, 1 ppm, and 10 ppm H_2S gas at room temperature.

Figure 4.4a shows the dynamic response of pure WO_3, pure NiO and WO_3-NiO nanowire composites towards 10 ppm H_2S measured at room temperature. The bare NiO nanowires do not indicate any response against 10 ppm H_2S, which is the same as the sensing results described in

Chapter 3. The sensing response was enhanced significantly for W3N1. Due to the high molar ratio of WO_3 to NiO, the WO_3-NiO nanocomposites show n-type gas sensing behavior towards reducing H_2S gas. The sensing response decrease as the molar ratio of NiO increases further. This can be explained as the increase of the non-responsive insulating layer of NiO on the surface of WO_3.

Figure 4.5 shows the comparative response% performance for the W3N1 gas sensor towards H_2S, CO, C_6H_6 and NH_3. An excellent response% and selectivity performance towards H_2S is found as compared with other interfering gases.

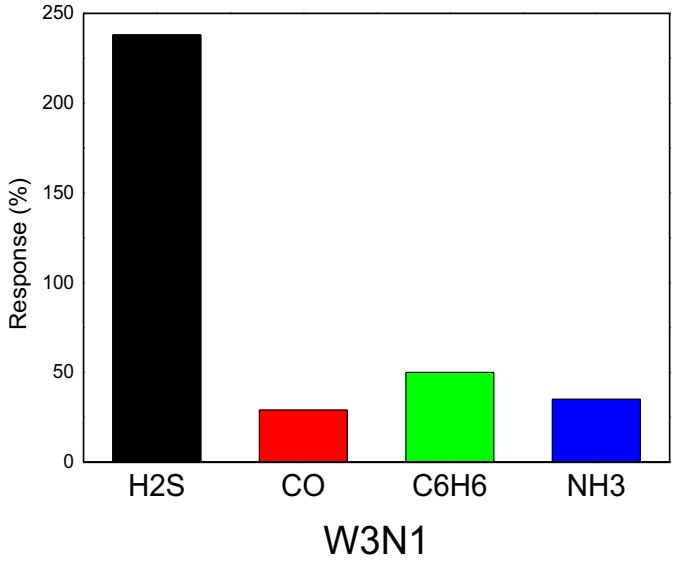

Figure 4.5 Comparative response % performance for W3N1 towards 10 ppm H_2S, CO, C_6H_6 and NH_3.

4.4 Mechanisms for enhanced sensing performance

The SEM morphology of the WO_3-NiO nanocomposite is shown in Figure 4.6a. As discussed in Chapter 2, the average diameter of NiO is much smaller (~10 nm) than that of WO_3 (~70 nm). Figure 4.6a indicates that the relatively smaller NiO nanowires are decorated on the

WO_3 nanowire surface. The respective schematic model is also shown in Figure 4.6b. There are three different conductive pathways to control the sensing mechanism, namely n-n junction (WO_3- WO_3), n-p junction (WO_3-NiO), and p-p junction (NiO-NiO). As pure NiO is resistive and has no role to control the sensing mechanism, the sensing mechanism is mostly controlled by the comparatively conductive n-n homo-junction (Figure 4.7a and b) and n-p hetero-junction path (Figure 4.6a and b).

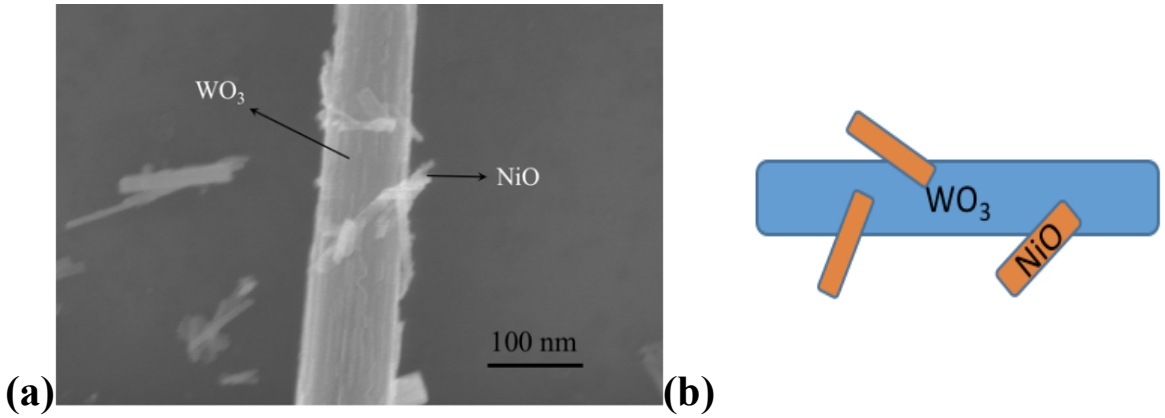

Figure 4.6 (a) SEM images of the W3N1 nanocomposite and (b) schematic illustration for the connection between WO_3 and NiO.

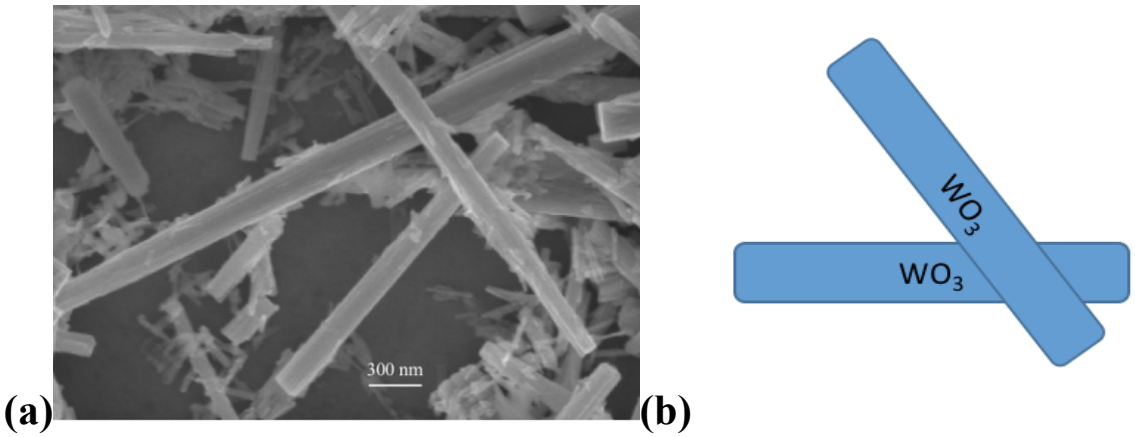

Figure 4.7 (a) SEM images of the W3N1 nanocomposite and (b) schematic illustration for the connection between WO_3 and WO_3 nanowires.

The basic sensing mechanism of the p-n junction can be explained as follows: when the Fermi energy (E_f) of one metal oxide semiconductor material is different from the other after the connection of these two kinds of materials, the electrons will flow across the grain interface to an unoccupied lower-energy state until the Fermi energies have equilibrated. This causes the electrons and holes recombination near the interface. This whole process will lead to the formation of a depletion area across the interface and also cause the band bending in this area, which means the carrier transfer channel becomes narrower. The schematic illustration of this process is indicated in Figure 4.8.

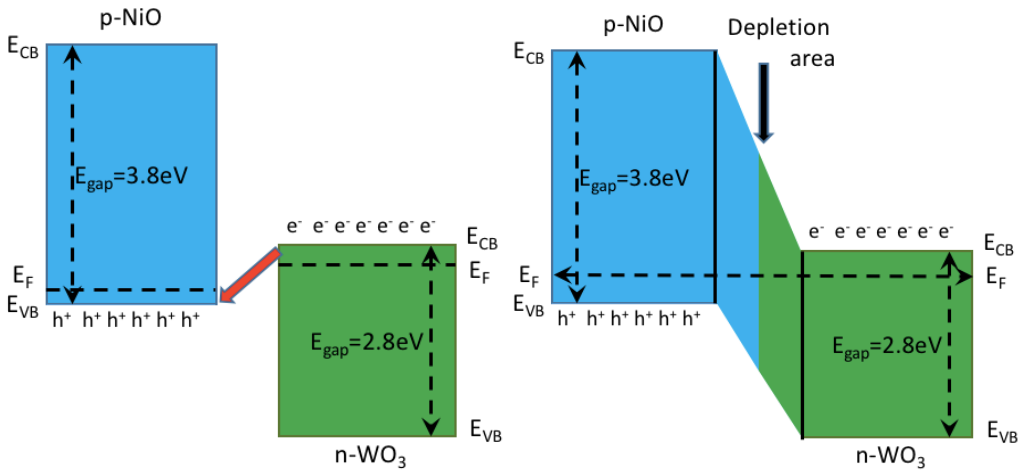

Figure 4.8 Schematic illustration of the formation of p-n junction between n-type WO_3 and p-type NiO

Considering the specific situation in our thesis, the gas sensing behavior of WO_3-NiO nanocomposites towards H_2S gas can be attributed to two reasons. First, the Fermi energy level of WO_3 is higher than that of NiO, which means the electrons will flow from n-type WO_3 nanowires to p-type NiO. That will lead to the formation of the potential energy barrier at the interface and an increase in the resistance of WO_3 due to the decrease of electrons density inside. The formation of the adsorbed oxygen ion at the surface of the WO_3 nanowire increased the

resistance more. When the typical reducing gas H_2S is introduced into the chamber, a large decrease in the resistance is possible due to the change in the large potential barrier at the hetero-interface.

4.5 Summary and conclusion

In this chapter we have fabricated Ag-doped WO_3 nanowire gas sensors and WO_3-NiO nanocomposite gas sensors. For the silver nanoparticle-decorated WO_3 sensors, we have demonstrated the gas sensing performance at room temperature for H_2S. From the data analysis we have optimized the molar ratio of WO_3 to Ag NPs with respect to sensitivity, recovery and response time. The WO_3/Ag (molar ratio 100:1) sensor showed better sensitivity than pure WO_3. A fast sensing response and recovery were also achieved by the decoration of Ag NPs on WO_3 nanowires. The Ag NPs work as the dominant active sites for H_2S adsorption in the sensing process. However, for a higher molar concentration of Ag, the sensor conductivity mechanism is significantly controlled by the metallic nature of silver and thus the sensitivity drops.

With regard to the WO_3-NiO nanocomposite gas sensor, we have characterized the gas sensing performance for CO, H_2S and C_6H_6 at room temperature under different molar ratios of WO_3 to NiO. We have optimized the sensitivity and selectivity performance samples to H_2S with a specific molar ratio (W3N1). These nano-composites samples indicated extraordinary sensitivity compared to most of the reported sensors, including the WO_3/Ag (molar ratio 100:1) sensors to H_2S at room temperature. The formation of a p-n junction between WO_3 and NiO caused by a difference in Fermi energy could explain the enhancement in sensitivity. To improve the recovery time of this kind of sensor, further research is still need.

CHAPTER 5 SUMMARY AND CONCLUSION

5.1 Metal oxide nanowires for gas sensing applications

The gas sensing and structural properties of bare NiO, ZnO, WO_3 and TiO_2 were investigated. The sensing performance of these metal oxide nanowires to H_2S, CO, NH_3 and NO_2 at room temperature was also investigated. From the sensing data, we have found that ZnO and NiO showed the optimum, selective performance towards the ppm level NO_2 (1 ppm) among other target gases such as H_2S, CO and NH_3.

The comparison of room temperature NO_2 sensing performance in literature with the present study based on ZnO and NiO nanowire is shown in Table 5.1. From the table, we can find that the sensing properties of ZnO and NiO are good among these different gas sensing materials. The gas sensing application of these metal oxide nanowires needs further investigation towards other air pollutant gases such as C_6H_6, formaldehyde and so on.

Table 5.1 Comparison of sensing performance with literature for NO_2 sensing at room temperature.

Materials	Sensitivity	Response time	Recovery time	Concentration	Reference
ZnO NWs	66.7%	160s	>300s	1ppm	This work
NiO NWs	58.7%	220s	>300s	1ppm	This work
RGO	11.1%	1080s	>1800s	2ppm	62
PPy/α-Fe2O_3	54%	89s	4205s	100ppm	63
ZnSe NWs	2%	150s	200s	1ppm	64
WO_3 films	80%	900s	2800s	5ppm	65

5.2 WO_3/Ag and WO_3-NiO composites for hydrogen sulfide sensing

Silver-doped WO_3 gas sensors were fabricated and demonstrated for H_2S sensing at room temperature. The doped gas sensors show the best sensing performance at a specific molar ratio of WO_3 to Ag. The hetero-structure nanocomposites of WO_3-NiO with different molar ratios have been fabricated and demonstrated for room temperature H_2S gas sensors. The gas sensor with the molar ratio of WO_3 to NiO of 1:3 indicates the optimum, selective sensing response against H_2S among other gases. The comparison of the materials for H_2S gas sensing at room temperature is listed in Table 5.2.

A comparison of room temperature H_2S sensing performance in literature with the present study based on WO_3/Ag and WO_3-NiO nanocomposites is shown in Table 5.2. From the table we can find that the sensitivity of the WO_3-NiO composite is better than most other sensors, and WO_3/Ag sensors also exhibit good sensitivity and response time.

Table 5.2 Comparison of sensing performance with literatures for H_2S sensing at room temperature.

Materials	Sensitivity	Response time	Recovery time	Concentration	Reference
WO_3/Ag(1/100)	78%	125s	540s	10ppm	This work
WO_3-NiO(3-1)	235%	270s	>600s	10ppm	This work
ZnOnanorods flower-like	99%	320s	3592s	5ppm	66
In_2O_3	35%	48s	50s	10ppm	67
TeO_2	7%	500s	800s	100ppm	68

A significant contribution of Ag nanoparticles and p-type NiO nanowires to the WO_3 nanowire-based gas sensor is their capability to tune the sensing properties at room temperature.

For example, hybrids of Ag NP-decorated WO_3 exhibit enhanced sensitivity, response and recovery to H_2S. WO_3-NiO nano-composites show selectivity for sensing H_2S.

REFERENCES

1. Choi, K. J., & Jang, H. W. (2010). One-Dimensional Oxide Nanostructures as Gas-Sensing Materials: Review and Issues, 4083–4099.

2. Comini, E., &Comini, E. (2016). Metal Oxide Nano-Crystals for Gas Sensing Metal oxide nano-crystals for gas sensing, (January).

3. Choopun, S., Wongrat, E., &Hongsith, N. (2012). Metal-oxide nanowires for gas sensors. Metal oxide Nanowires for Gas Sensors, (Cvd), 3–24.

4. Kim, J., & Yong, K. (2011). Mechanism Study of ZnONanorod-Bundle Sensors for H2S Gas Sensing. *The Journal of Physical Chemistry C*, 115(15), 7218–7224.

5. Su, P. G., & Peng, Y. T. (2014). Fabrication of a room-temperature H2S gas sensor based on PPy/WO3 nanocomposite films by in-situ photopolymerization. *Sensors and Actuators, B: Chemical*, 193, 637–643.

6. Guidotti, T. L. (2010). Hydrogen sulfide: advances in understanding human toxicity. *International Journal of Toxicology*, 29(6), 569–581.

7. Kwon, J., Shim, H., Lim, D., Kang, K., Lee, J., Kim, K., & Kim, S. (2010). A study on detecting amine gas using chemical characterization of Ag nanowire. 2010 10th IEEE Conference on Nanotechnology, NANO 2010, 753–757.

8. Goldstein M (December 2008). "Carbon monoxide poisoning". Journal of Emergency Nursing: JEN: Official Publication of the Emergency Department Nurses Association 34 (6): 538–542.

9. Threshold Limit Values (TLV) and Immediately Dangerous to Life and Health (IDLH) values. (2005). *Safety And Health*, 900.

10. Liu, P., He, K., Li, Y., Wu, Q., Yang, P., & Wang, D. (2012). Exposure to mercury causes formation of male-specific structural deficits by inducing oxidative damage in nematodes. Ecotoxicology and Environmental Safety, 79, 90–100.

11. Zampolli, S., Elmi, I., Strmann, J., Nicoletti, S., Dori, L., &Cardinali, G. C. (2005). Selectivity enhancement of metal oxide gas sensors using a micromachined gas chromatographic column. *Sensors and Actuators, B: Chemical,* 105(2), 400–406.

12. Muksunov, T. R., Maksimova, N. K., Sevast'yanov, E. Y., Shipilov, S. É., &Yakubov, V. P. (2015). Increase in the Sensitivity and Selectivity of Semiconductor Gas Sensors. *Russian Physics Journal*, 57(9), 1287–1293.

13. Eu, K. S., & Yap, K. M. (2014). Overcoming Long Recovery Time of Metal-Oxide Gas Sensor With Certainty Factor Sensing Algorithm. *Proceedings of the 8th International Conference on Sensing Technology*, 2–4.

14. Choi, K. J., & Jang, H. W. (2010). One-Dimensional Oxide Nanostructures as Gas-Sensing Materials: Review and Issues, 4083–4099.

15. Wang, C., Yin, L., Zhang, L., Xiang, D., & Gao, R. (2010). Metal oxide gas sensors: Sensitivity and influencing factors. *Sensors*, 10(3), 2088–2106.

16. Miller, D. R., Akbar, S. A., & Morris, P. A. (2014). Nanoscale metal oxide-based heterojunctions for gas sensing: A review. *Sensors and Actuators, B: Chemical,* 204, 250–272.

17. http://www.who.int/mediacentre/news/releases/2014/air-pollution/en/

18. Filipovic, L., &Selberherr, S. (2015). Performance and Stress Analysis of Metal Oxide Films for CMOS-Integrated Gas Sensors. *Sensors*, 15(4), 7206–7227.

19. KyoungJin Choi, Ho Won Jang. 2010. One-dimensional oxide nanostructures as gas sensing materials: review and issues. *Sensors*. 10: 4083-4099.

20. N. Yamazoe. 1991. New approaches for improving semiconductor gas sensors, *Sensors and Actuators B: Chemical*. 5: 7–19.

21. Sun, Y.-F., Liu, S.-B., Meng, F.-L., Liu, J.-Y., Jin, Z., Kong, L.-T., & Liu, J.-H. (2012). Metal Oxide Nanostructures and Their Gas Sensing Properties: A Review. Sensors, 12(3), 2610–2631.

22. Wang, C., Chu, X., & Wu, M. (2006). Detection of H2S down to ppb levels at room temperature using sensors based on ZnOnanorods. *Sensors and Actuators, B: Chemical*, 113(1), 320–323.

23. Kaur, M., Bhattacharya, S., Roy, M., Deshpande, S. K., Sharma, P., Gupta, S. K., &Yakhmi, J. V. (2007). Growth of nanostructures of Zn/ZnO by thermal evaporation and their application for room-temperature sensing of H 2 S gas. *Applied Physics A: Materials Science and Processing,* 87(1), 91–96.

24. Chen, J., Wang, K., Hartman, L., & Zhou, W. (2008). Supporting Information H2S Detection by Vertically Aligned CuO Nanowire Array Sensors. *Materials Research*, 2–3.

25. Ghimbeu, C. M., Schoonman, J., Lumbreras, M., &Siadat, M. (2007). Electrostatic spray deposited zinc oxide films for gas sensor applications. *Applied Surface Science*, 253(18), 7483–7489.

26. Chaudhari, G. N., Bambole, D. R., Bodade, A. B., &Padole, P. R. (2006). Characterization of nanosized TiO2 based H2S gas sensor. *Journal of Materials Science*, 41(15), 4860–4864.

27. Law, M., Kind, H., Messer, B., Kim, F., & Yang, P. (2002). Photochemical Sensing of NO2 with SnO_2 NanoribbonNanosensors at Room Temperature. *AngewandteChemie International Edition*, 41(13), 2405–2408.

28. Ponzoni, A., Comini, E., Sberveglieri, G., Zhou, J., Deng, S. Z., Xu, N. S., … Wang, Z. L. (2006). Ultrasensitive and highly selective gas sensors using three-dimensional tungsten oxide nanowire networks. *Applied Physics Letters*, 88(20), 29–31.

29. Kim, I. D., Rothschild, A., Lee, B. H., Kim, D. Y., Jo, S. M., &Tuller, H. L. (2006). Ultrasensitive chemiresistors based on electrospunTiO 2 nanofibers. *Nano Letters*, 6(9), 2009–2013.

30. Sadek, A. Z., &Wlodarski, W. (2005). ZnONanobelt Based Conductometric H2 and NO2 Gas Sensors, (2), 1326–1329.

31. Rout, C. S., Ganesh, K., Govindaraj, A., & Rao, C. N. R. (2006). Sensors for the nitrogen oxides, NO2, NO and N2O, based on In2O3 and WO3 nanowires. *Applied Physics A: Materials Science and Processing*, 85(3), 241–246.

32. Liao, L., Mai, H. X., Yuan, Q., Lu, H. B., Li, J. C., Liu, C., … Yu, T. (2008). Single CeO2 nanowire gas sensor supported with Pt nanocrystals: Gas sensitivity, surface bond states, and chemical mechanism. *Journal of Physical Chemistry C*, 112(24), 9061–9065.

33. Kolmakov, A., Zhang, Y., Cheng, G., &Moskovits, M. (2003). Detection of CO and O2 using tin oxide nanowire sensors. *Advanced Materials*, 15(12), 997–1000.

34. Susanti, D., Diputra, A. A. G. P., Tananta, L., Purwaningsih, H., Kusuma, G. E., Wang, C., Huang, Y. (2014). WO3 nanomaterials synthesized via a sol-gel method and calcination for use as a CO gas sensor. *Frontiers of Chemical Science and Engineering*, 8(2), 179–187.

35. Wagh, M. S., Jain, G. H., Patil, D. R., Patil, S. A., &Patil, L. A. (2006). Modified zinc oxide thick film resistors as NH_3 gas sensor. *Sensors and Actuators, B: Chemical*, 115(1), 128–133.

36. Ponzoni, A., Comini, E., Sberveglieri, G., Zhou, J., Deng, S. Z., Xu, N. S., … Wang, Z. L. (2006). Ultrasensitive and highly selective gas sensors using three-dimensional tungsten oxide nanowire networks. *Applied Physics Letters*, 88(20), 29–31.

37. Wang, J., Wei, L., Zhang, L., Jiang, C., Siu-Wai Kong, E., & Zhang, Y. (2012). Preparation of high aspect ratio nickel oxide nanowires and their gas sensing devices with fast response and high sensitivity. *Journal of Materials Chemistry*, 22(17), 8327.

38. Zhang, J., Liu, X., Neri, G., & Pinna, N. (2016). Nanostructured Materials for Room-Temperature Gas Sensors, 795–831.

39. Wang, Y., Jiang, X., & Xia, Y. (2003). A Solution-Phase, Precursor Route to Polycrystalline SnO2 Nanowires That Can Be Used for Gas Sensing under Ambient Conditions. *Journal of the American Chemical Society*, 125(52), 16176–16177.

40. Du, N., Zhang, H., Chen, B., Xiangyang, M., Liu, Z., Wu, J., & Yang, D. (2007). Porous indium oxide nanotubes: Layer-by-layer assembly on carbon-nanotube templates and application for room-temperature NH3 gas sensors. *Advanced Materials*, 19(12), 1641–1645.

41. Xiao-Ying, W. Y.-Q. and H. M. and W. (2014). A study of transition from n- to p-type based on hexagonal WO 3 nanorods sensor. *Chinese Physics B*, 23(4), 40704.

42. Wang, C., Chu, X., & Wu, M. (2006). Detection of H2S down to ppb levels at room temperature using sensors based on ZnOnanorods. *Sensors and Actuators, B: Chemical*, 113(1), 320–323.

43. Lupan, O., Ursaki, V. V., Chai, G., Chow, L., Emelchenko, G. A., Tiginyanu, I. M., Redkin, A. N. (2010). Selective hydrogen gas nanosensor using individual ZnO nanowire with fast response at room temperature. *Sensors and Actuators, B: Chemical*, 144(1), 56–66.

44. Chang, S.-J., Hsueh, T.-J., Chen, I.-C., & Huang, B.-R. (2008). Highly sensitive ZnO nanowire CO sensors with the adsorption of Au nanoparticles. Nanotechnology, 19(17), 175502.

45. Chang, C.-M., Hon, M.-H., &Leu, I.-C. (2012). Improvement in CO sensing characteristics by decorating ZnOnanorod arrays with Pd nanoparticles and the related mechanisms. *RSC Advances*, 2, 2469.

46. Ramgir, N. S., Mulla, I. S., &Vijayamohanan, K. P. (2005). A room temperature nitric oxide sensor actualized from Ru-doped SnO 2 nanowires. *Sensors and Actuators, B: Chemical*, 107(2), 708–715.

47. Gong, J., Chen, Q., Lian, M. R., Liu, N. C., Stevenson, R. G., &Adami, F. (2006). Micromachinednanocrystalline silver doped SnO2 H2S sensor. *Sensors and Actuators, B: Chemical*, 114(1), 32–39.

48. Ma, J., Liu, Y., Zhang, H., Ai, P., Gong, N., Wu, Y., & Yu, D. (2015). Room temperature ppb level H2S detection of a single Sb-doped SnO2 nanoribbon device. *Sensors and Actuators B: Chemical*, 216, 72–79.

49. Zong, Y., Cao, Y., Jia, D., Bao, S., & Lu, Y. (2010). Facile synthesis of Ag/ZnOnanorods using Ag/C cables as templates and their gas-sensing properties. *Materials Letters*, 64(3), 243–245.

50. Jimenez, I., Centeno, M. a., Scotti, R., Morazzoni, F., Arbiol, J., Cornet, a., &Morante, J. R. (2004). NH3 interaction with chromium-doped WO3 nanocrystalline powders for gas sensing applications. *Journal of Materials Chemistry*, 14(15), 2412.

51. T. B. Fryberger and S. Semancik,. Model studies of SnO2-based gas sensors: vacancy defects and Pd additive effects. *Sens. Actuators*, 2, 305 (1990).

52. Mädler, L., Roessler, A., Pratsinis, S. E., Sahm, T., Gurlo, A., Barsan, N., & Weimar, U. (2006). Direct formation of highly porous gas-sensing films by in situ thermophoretic deposition of flame-made Pt/SnO 2 nanoparticles. *Sensors and Actuators, B: Chemical,* 114(1), 283–295.

53. Choi, U. S., Sakai, G., Shimanoe, K., &Yamazoe, N. (2005). Sensing properties of Au-loaded SnO2-Co3O4 composites to CO and H2. *Sensors and Actuators, B: Chemical,* 107(1 SPEC. ISS.), 397–401.

54. Chen, D., Yin, L., Ge, L., Fan, B., Zhang, R., Sun, J., & Shao, G. (2013). Low-temperature and highly selective NO-sensing performance of WO 3 nanoplates decorated with silver nanoparticles. *Sensors and Actuators, B: Chemical*, 185, 445–455

.

55. Na, C. W., Woo, H., & Lee, J. (2012). Highly sensitive VOC sensors using NiO-decorated ZnO nanowire networks: the effect of radial p-n junction, (1), 694–696.

56. Wang, L., Kang, Y., Wang, Y., Zhu, B., Zhang, S., Huang, W., & Wang, S. (2012). CuO nanoparticle decorated ZnOnanorod sensor for low-temperature H 2S detection. *Materials Science and Engineering C*, 32(7), 2079–2085.

57. Patil, D. R., Patil, L. a., &Patil, P. P. (2007). Cr2O3-activated ZnO thick film resistors for ammonia gas sensing operable at room temperature. *Sensors and Actuators B: Chemical*, 126(2), 368–374.

58. Somacescu, S., Dinescu, A., Stanoiu, A., Simion, C. E., & Calderon Moreno, J. M. (2012). Hydrothermal synthesis of ZnO–Eu2O3 binary oxide with straight strips morphology and sensitivity to NO2 gas. *Materials Letters*, 89, 219–222.

59. Choopun, S., Wongrat, E., &Hongsith, N. (2012). Metal-oxide nanowires for gas sensors. *Metal -Oxide Nanowires for Gas Sensors*, (Cvd), 3–24.

60. http://li155-94.members.linode.com/myscope/sem/practice/principles/layout.php

61. X-ray, P. (n.d.). Powder X-ray Diffraction Powder X-ray Diffraction Bragg ' s Law, 1–4.

62. Lu, G., Ocola, L. E., & Chen, J. (2009). Reduced graphene oxide for room-temperature gas sensors. *Nanotechnology*, *20*(44), 445502.

63. Navale, S. T., Khuspe, G. D., Chougule, M. A., &Patil, V. B. (2014). Room temperature NO2 gas sensor based on PPy/α-Fe2O3 hybrid nanocomposites. *Ceramics International*, *40*(6), 8013–8020.

64. Park, S., Kim, S., Lee, W. I., Kim, K.-K., & Lee, C. (2014). Room temperature, ppb-level NO\n 2\n gas sensing of multiple-networked ZnSe nanowire sensors under UV illumination. *Beilstein Journal of Nanotechnology*, *5*(2), 1836–1841.

65. Su, P. G., & Pan, T. T. (2011). Fabrication of a room-temperature NO2 gas sensor based on WO3 films and WO3/MWCNT nanocomposite films by combining polyol process with metal organic decomposition method. *Materials Chemistry and Physics*, *125*(3), 351–357.

66. Hosseini, Z. S., Zad, a. I., &Mortezaali, a. (2015). Room temperature H2S gas sensor based on rather aligned ZnOnanorods with flower-like structures. *Sensors and Actuators B: Chemical*, *207*, 865–871.

67. Zeng, Z., Wang, K., Zhang, Z., Chen, J., & Zhou, W. (2009). The detection of H2S at room temperature by using individual indium oxide nanowire transistors. *Nanotechnology*, *20*(4), 045503.

68. Liu, Z., Yamazaki, T., Shen, Y., Kikuta, T., Nakatani, N., & Kawabata, T. (2007). Room temperature gas sensing of p -type Te O2 nanowires. *Applied Physics Letters*, *90*(17), 2–5.